Macrophage crosstalk with neural progenitors and fibroblasts controls regenerative neurogenesis via Sema4ab after spinal cord injury in zebrafish

Alberto Docampo-Seara[1], Mehmet Ilyas Cosacak[1§], Kim Heilemann[1§], Friederike Kessel[1], Ana-Maria Oprişoreanu[1], Özge Çark[1], Daniela Zöller[1], Josi Arnold[1], Anja Bretschneider[1], Alisa Hnatiuk[1], Nikolay Ninov[1], Catherina G. Becker[1,2,3]*, Thomas Becker[1,2]*

1 Center for Regenerative Therapies Dresden at the TU Dresden, Fetscherstraße 105, 01307 Dresden, Germany

2 Centre for Discovery Brain Sciences, University of Edinburgh Medical School: Biomedical Sciences, Edinburgh EH16 4SB, UK

3 Cluster of Excellence Physics of Life, TU Dresden, 01062 Dresden, Germany

§ equal contribution

* Senior author

Key words: spinal cord regeneration, cell-cell interactions, scRNAseq, neurogenesis, macrophages, fibroblasts, *tgfb3, sema4a*

ABSTRACT

After spinal cord injury, interactions of multiple tissues inhibit neuronal regeneration in mammals, but not in anamniotes, such as zebrafish. These pivotal interactions are poorly understood. Here we analyse the role of the cell signalling molecule *sema4ab* in the cell communication network leading to regenerative neurogenesis after spinal injury in larval zebrafish. *Sema4ab* is expressed by macrophages and gene ablation doubles the rate of regenerative neurogenesis. Disruption of the *sema4ab* receptor *plxnb1a/b*, expressed by spinal progenitor cells, also moderately increases regenerative neurogenesis. In addition, single cell transcriptomics reveals altered interactions between macrophages and multiple additional cell types after *sema4ab* disruption. Pro-inflammatory cytokines are down-regulated and fibroblasts upregulate expression of the anti-inflammatory cytokine *tgfb3.* Inhibition of *tgfb3* abolishes effects of *sema4ab* disruption on regenerative neurogenesis. This highlights *sema4ab* as a direct and indirect inhibitor of regenerative neurogenesis and as a potential therapeutic target in non-regenerating mammals.

INTRODUCTION

Mammals, including humans, fail to regenerate neurons lost to protracted secondary cell death around a spinal injury site (Dusart & Schwab, 1994; Liu *et al*, 1997). Spinal progenitor cells can generate new neurons in a conducive environment and can even be re-programmed *in vivo* to produce some favourable cell types for regeneration, such as oligodendrocytes, but not neurons (Llorens-Bobadilla *et al*, 2020; Shihabuddin *et al*, 2000; Stenudd *et al*, 2022). The inhibitory environment in a spinal injury site is highly complex, consisting of invading immune cells, such as macrophages, glial cells, such as astrocytes, and stromal cells, such as fibroblasts. Interactions of these cell types result in an inhibitory environment for regeneration in which prolonged inflammation, as well as fibrotic and astrocytic scarring predominates (Anderson et al., 2016; Dias et al., 2018; Francos-Quijorna et al., 2022; Kroner et al., 2014).

In contrast, zebrafish functionally regenerate their spinal cord at the adult and larval stage (Becker *et al*, 2004; Chang *et al*, 2021; Mokalled *et al*, 2016; Ohnmacht *et al*, 2016; Vandestadt *et al*, 2021). This includes regeneration of new neurons from resident progenitors (Briona & Dorsky, 2014; Briona *et al*, 2015; Huang *et al*, 2021; Ohnmacht *et al.*, 2016; Reimer *et al*, 2008). In zebrafish, these cells are termed ependymo-radial glial cells (ERGs), by virtue of their combination of ependymal and astroglial features (Becker & Becker, 2015).

In a spinal injury site in zebrafish, blood-derived macrophages have been shown to directly signal to progenitor cells to promote regeneration of neurons, for example by direct tumour necrosis factor (Tnf) signalling to specific

receptors on ERGs (Cavone *et al*, 2021). Macrophages also control the number of pro-inflammatory neutrophils and overall levels of Il1b, a major pro-inflammatory cytokine, suggesting that these cells interact with a variety of cell types to condition the injury site (Tsarouchas *et al*, 2018). Macrophages/microglia and astrocyte-like cells produce a range of regeneration-promoting growth factors in central nervous system (CNS) injuries in zebrafish (Cigliola *et al*, 2023; Goldshmit *et al*, 2012; Kyritsis *et al*, 2012; Mokalled *et al.*, 2016). Moreover, fibroblasts that invade a spinal lesion site, promote regeneration by producing favourable extracellular matrix components for axonal regeneration (Kolb *et al*, 2023; Tsata *et al*, 2021; Wehner *et al*, 2017). Hence, the cellular composition of the injury site comprises a number of interacting cell types that are relevant to the regenerative process. How the interplay of neural and non-neural cell types in fish leads to a different outcome to that in mammals is not well understood, but could give important insights into potential roadblocks of CNS regeneration in mammals.

To understand how macrophages condition the lesion site environment, we analysed the role of the conserved signalling molecule Semaphorin 4A (Sema4A) in macrophages. *sema4a* is mainly expressed by macrophages and microglial cells and can change their activation state (Leitner *et al*, 2015; Meda *et al*, 2012), putting the gene into a position to affect several post-injury events. For example, Sema4a has been shown to promote a pro-fibrotic phenotype in fibroblasts in vitro, suggesting possible interactions with fibroblasts (Carvalheiro *et al*, 2019). This immune semaphorin can signal bi-directionally in its transmembrane configuration or can be released as a soluble signalling molecule to act on plexin receptors (Rajabinejad *et al*, 2020; Sun *et al*, 2017).

Interestingly, knock out of the principal Sema4A receptors Plexin B1 and B2 impairs neurogenesis in the developing mouse brain (Daviaud *et al*, 2016). These observations suggest that Sema4a could have multiple roles in a spinal injury site.

Here, we find that a zebrafish orthologue of Sema4A, *semaphorin4ab (sema4ab)* is expressed primarily by macrophages in a spinal injury site, a pattern that is conserved in mice. Even though the larval spinal cord shows regenerative neurogenesis, *sema4ab* attenuates this process through complex tissue interactions after spinal cord injury in zebrafish larvae, which may regulate self-renewal and/or differentiation of progenitors. We show that this signalling likely occurs directly via *plxnb1a/b,* expressed in progenitor cells. We also provide evidence by single cell transcriptomics that *sema4ab* modulates interactions of multiple other cell types. In particular, *sema4ab* controls production of the pro-regenerative factor *tgfb3* by fibroblasts. Overall, we show that *sema4ab* expressing macrophages orchestrate regenerative neurogenesis directly by signalling to ERGs and indirectly by attenuating expression of pro-regenerative signals in fibroblasts.

RESULTS

Sema4ab is expressed mainly in macrophages during regeneration

After a complete spinal lesion at 3 days post-fertilization (dpf), lesion-induced neurogenesis peaks at 24 hours post-lesion (hpl) in larval zebrafish. Axons have regrown over the lesion site and swimming function is largely recovered by 48 hpl (Ohnmacht *et al.*, 2016; Wehner *et al.*, 2017). Thus, major regenerative processes occur within 48 hpl. We analysed the expression pattern of the potentially macrophage-activation related gene *sema4ab* in whole-mount larvae by multiplexed hybridization chain reaction fluorescence *in situ* hybridization (HCR-FISH) during that time period in reporter fish for macrophages, comprising blood-derived macrophages and microglia (*mpeg:mCherry)*, in which mCherry is expressed under the *mpeg1.1* promoter (Ellett *et al*, 2011), and in reporter fish for neutrophils (*mpx:GFP*), in which GFP is expressed under the *mpx* promoter (Renshaw *et al*, 2006) .

At 3 dpf, hardly any macrophages, neutrophils or other *sema4ab*+ cells were observed in the intact spinal cord. At 6 hpl, numbers of *sema4ab*+ cells were strongly increased surrounding the lesion site (Fig. 1A-B; see Suppl. Fig. 1A for method control). Of these cells, 65 % were positive for *mpeg:mCherry*, indicating expression in macrophages. At 24 hpl and at 48 hpl, numbers of *sema4a*+ cells in the lesion site remained high. At 24 hpl, 85 % and at 48 hpl, 75 % of all *sema4ab*+ *cells* were macrophages (*mpeg:mCherry+)*. In turn, of all macrophages, 89 % were *sema4ab*+ at 6 hpl, 84 % at 24 hpl and 72 % at 48 hpl (Fig. 1C-D). Hence most macrophages in the lesion site are *sema4ab*+ and represent the major cell population in the lesion site to express the gene.

Co-labelling of *sema4ab* with *mpx:GFP* expressing neutrophils indicated no signal in the spinal cord of unlesioned larvae at 3 dpf. After lesion, numbers of neutrophils were increased in the lesion site. 16 % of neutrophils were *sema4ab*+ at 6 hpl and at 24 hpl (Suppl. Fig 1B-D), indicating that the few *sema4ab*+ cells not labelled by the macrophage marker were likely mostly neutrophils.

To determine whether any of the *sema4ab* expressing macrophages (*mpeg:mCherry*+) were microglia, we used the microglial marker *apoeb* (Thiel et al., 2022) in triple labelling experiments. Indeed, we observed a population of *mpeg:mCherry*+/*sema4ab*+/apoeb+ cells in the centre of the lesion site at 24 hpl (Suppl. Fig. 1E). Around 60 % of total *mpeg:mCherry*+/ apoeb+ cells were also positive for *sema4ab,* indicating that microglial cells expressed *sema4ab* (Suppl. Fig. 1F-G). In summary, a spinal lesion induced the presence of *sema4ab*+ immune cells, with few if any non-immune cells expressing the gene in the lesion site. The vast majority of *sema4ab*+ immune cells were macrophages and microglial cells.

***Sema4ab* disruption increases regenerative neurogenesis.**

For a loss-of-function analysis of *sema4ab* in regenerative neurogenesis, we used acute injection of highly active sCrRNAs (haCRs) targeting *sema4ab* (Keatinge *et al*, 2021) and generated a stable germline mutant from haCR-injected fish. The germline mutant introduced a 14 bp insertion in exon 6, leading to a premature stop codon (Supp Fig. 2A), predicted to lead to a truncated protein lacking functionally important domains, such as sema superfamily domains, plexin repeat domains and the intracellular part, containing a sema4F domain (Suppl. Fig. 2A). Somatic mutants (Suppl. Fig. 2B-

C) showed no differences in growth compared to control gRNA injected larvae, as measured by body length (Suppl. Fig. 2D), notochord thickness (Suppl. Fig. 2E), or spinal cord thickness (Suppl. Fig. 2F). However, a small decrease in eye size was observed (8 % reduction, Suppl. Fig. 2G) that may be related to compromised photoreceptor maintenance in the absence of Sema4a function (Toyofuku *et al*, 2012). Similarly, germline mutants (Suppl. Fig. 2H-I) showed an unchanged body length compared to wild type fish (Suppl. Fig. 2J) and also a small reduction in eye diameter (9 % reduction; Suppl. Fig. 2K). Adults were viable and fertile. Hence, gross development of larvae is largely unimpaired in the absence of *sema4ab*.

To analyse regenerative neurogenesis, we used 5-Ethynyl-2'-deoxyuridine (EdU) labelling in the *mnx1:GFP* transgenic line that labels motor neurons. Motor neurons represent the main cell type that is newly generated during lesion-induced neurogenesis (Cavone et al., 2021). In unlesioned *sema4ab* haCR-injected larvae (EdU added at 72 hpf, analysis at 96 hpf, Fig. 2A) few newly generated motor neurons (EdU+/*mnx1*:*GFP*+) were present, similar to control gRNA-injected larvae. This was expected, since *sema4ab* was not detectable in the spinal cord without lesion (Fig. 2B) and shows that *sema4ab* does not have an important role in ongoing low-level developmental neurogenesis.

After a lesion at 3 dpf, we observed a ~4-fold lesion-induced increase in numbers of new motor neurons in control gRNA-injected larvae at 48 hpl, as previously reported (Ohnmacht et al., 2016). Remarkably, in *sema4ab* haCR injected larvae, this number was further increased by 85 % compared to lesioned wild type control gRNA-injected larvae (Fig. 2 D-F). Similarly, in the

lesioned *sema4ab* germline mutant, the number of new motor neurons almost doubled (95 % increase) compared to lesioned wild type control larvae (Fig. 2G). Hence, *sema4ab* strongly attenuates regenerative neurogenesis, but leaves developmental neurogenesis unaffected.

For a gain-of-function approach, we generated a construct that leads to overexpression of *sema4ab* and a fluorescent reporter under the control of a heat-shock promotor (*hsp70l:sema4ab-t2a-mcherry,* abbreviated as *hsp70:sema4ab*, Suppl. Fig. 3A). We observed reporter gene expression mainly in muscle cells in heat-shocked lesioned plasmid injected-fish but not in heat-shocked lesioned fish that did not receive plasmid injection (Suppl. Fig. 3B). qRT-PCR in heat-shocked plasmid-injected fish vs heat-shocked controls indicated up to 140 times increased mRNA levels that returned to baseline by 24 hours post-induction (Suppl. Fig. 3C-D).

We used multiple (4 hours before lesion, 20 hpl, 36 hpl) heat-shocks in lesioned animals to ensure sufficient levels of over-expressed *sema4ab* mRNA. However, we did not observe significant changes in regenerative neurogenesis as determined by the number of EdU+/*mnx1:GFP*+ cells at 48 hpl (Suppl. Fig. 3E,F). This suggested that the endogenous levels of *sema4ab* expression already had maximal effects on lesion-induced neurogenesis. In addition, this experiment shows that added Sema4ab protein is not toxic for neurogenesis.

Next, we used the same heat-shock regime on *sema4ab* germline mutants, in which functional endogenous *sema4ab* was not present (Fig. 2H). Over-expression completely abolished the increased lesion-induced neurogenesis seen in the mutant (Fig. 2I-J). Given that reporter expression for the overexpressed gene was only detectable in muscle cells, rescuing activity in

the spinal cord may be through signalling of soluble Sema4ab signalling from muscle cells. Moreover, this observation confirms that our *sema4ab* mutant carries a *loss-of-function* mutation and that Sema4ab controls regenerative neurogenesis.

Disruption of *plxnb1a/b* augments regenerative neurogenesis.

To gain mechanistic insight into the role of *sema4ab* in regenerative neurogenesis, we considered potential direct signalling from *sema4ab*+ macrophages to ERG progenitor cells. Such signalling would require specific receptors on ERGs. To find receptors that are expressed by ERGs, we re-analysed previous scRNAseq data on ERG-enriched samples (Cavone *et al.*, 2021). This highlighted potential expression of the two *plxnb1* (*plxnb1a*, *plxnb1b) and plxn2b* (*plxnb2a* and *plxnb2b)* paralogs that code for potential Sema4a receptors (Meda *et al.*, 2012; Rajabinejad *et al.*, 2020).

To validate the likely presence of these receptors, we performed HCR-FISH analysis on whole larvae using the *her4.1:EGFP* line, in which ERG progenitor cells are fluorescently labelled. Multiplexed HCR-FISH for *plxn1a and plxn1b* in the same larvae showed that *plxnb1a* mRNA was detectable at low levels in ERGs in unlesioned animals at 3 dpf, with no detectable increase at 24 hpl (Fig. 3A,B). The signal for *plxnb1b* was generally stronger than that for *plxnb1a*, and also did not show detectable changes after lesion (Fig. 3C). High magnifications indicated co-expression of *plxnb1a and plxnb1b* in the same ERGs (Fig. 3D). Only very low (*plxnb1a*) or no signal (*plxnb1b*) was detectable outside ERGs in the spinal cord for both *plxnb1a* and *plxnb1b.*

Selective expression of *plxnb1a* and *plxnb1b* in ERGs made these good candidates for receiving a *sema4ab* signal. Therefore, we disrupted *plxnb1a* and *plxnb1b* by haCR injection (Fig 3E,G). While single somatic mutations had no effect, simultaneous mutation of *plxnb1a* and *plxnb1b* by co-injecting the respective haCRs increased numbers of newly generated motor neurons (EdU+/mnx1:*GFP*+) by 55 % at 48 hpl.

plxnb2a was only detectable in cells that were located lateral to ERGs in unlesioned and lesioned animals, whereas *plxnb2b* was expressed in ERGs in unlesioned and lesioned larvae (Suppl. Fig. 4A-D). In the lesion site, signal could be detected that was likely related to non-neuronal cells for both *plxnb2a* and *plxnb2b.* Disrupting *plxnb2a* and *plxnb2b* with haCRs had no detectable effect on regenerative neurogenesis (Suppl. Fig 4E-G).

Hence, disrupting the potential sema4ab receptors *plxnb1a/b* partially replicated the effect of *sema4ab* mutation. This suggested direct macrophage to ERG interaction via Sema4ab signalling to Plxnb1 receptors on ERGs.

scRNAseq indicates changes in cell interactions between macrophages and other cell types

The observation that disruption of *plxnb1a/b* increased the number of newly generated motor neurons only by 55 % while in the *sema4ab* mutant their number was doubled raised the possibility of additional changes that may influence regenerative neurogenesis. To gain insight into these potential systemic changes in the lesion environment, we generated scRNAseq profiles to compare all cells in lesion site tissue from control gRNA-injected and *sema4ab* haCR-injected larvae at 24 hpl.

Per condition, 50 animals were pooled. Following quality control, removing doublets and low-quality cells (Suppl. Table 1), our scRNAseq experiments yielded 11788 cells for the control gRNA-injected sample (gControl). The sample from the *sema4ab* haCR injected animals was split into two technical repeats and yielded 11621 cells for sample 1 (gSema4abR1) and 11330 cells for sample 2 (gSema4abR2). Samples showed high similarities based on mean, median and total number of reads and genes detected per cells, indicating reproducibility of the experiments (Suppl. Table 2). Moreover, principal component analysis indicated that the two technical repeats of the *sema4ab* haCR treated condition were very closely related and more distant from the control sample (Suppl. Fig. 5A).To further validate the scRNAseq data, we tested three differentially expressed genes (*grn1*, 6.4-fold lower in somatic mutants; *irgl1l*, 7.46-fold higher in somatic mutants, and *adamts6*, 1.57-fold lower in somatic mutants) by qRT-PCR (Suppl. Fig. 5B). Results were aligned with differences in gene expression. Taken together, these observations indicate technical robustness of the scRNAseq data.

We validated the efficiency of the gene editing by quantifying the amplified target site for the *sema4ab* haCR from the scRNAseq data. In the control sample, we found 16.945 gene reads and 151 of these included haCR target site reads. The DNA base sequences of these were all correct. In contrast, in *sema4ab* haCR treated samples, we found the overall number of *sema4ab* reads reduced by more than a third (to 98880 and 10384 in technical replicates gSemaR1 and gSemaR2, respectively) and no intact reads of the haCR target site (Suppl. Table 3, see Suppl. Table 4 for example reads). This confirms high efficiency of gene disruption in this sample.

To determine potential biological effects of *sema4ab* disruption on the abundance of different cell types in the injury site, we performed unsupervised clustering of the data sets. This revealed 44 distinct cell clusters. Using previously established cell type-specific markers (see Material and Methods), we annotated these clusters and found that they fall into 15 major cell categories (Fig. 4A,B). We find that fibroblast-like cells constitute the majority of all cells (21.13 %), consisting of 7 clusters, followed by neural cells (14.86 %), consisting of ERGs, oligodendrocytes and 4 neuronal clusters, red blood cells (13.54 %), consisting of three clusters, muscle cells (13.54 %), consisting of 5 clusters, and immune cells (11.63 %), consisting of 4 macrophage and 2 neutrophil clusters. Hence, major cell types expected from histology were all represented in the samples. Importantly, comparing cell numbers between samples indicated no major changes in cell type representation resulting from *sema4ab* disruption (Fig. 4C, Suppl. Fig. 5C), with the possible exception of Peridermis cluster 2 (PD#2), which showed a ~50 % reduction in cell number. This suggests that *sema4ab* disruption did not lead to major shifts in cell type representation at a spinal injury site.

We next analysed possible changes in gene expression as a consequence of *sema4ab* disruption in the identified cell clusters. The two technical replicates of the *sema4ab* haCR-injected sample were integrated into one. All clusters showed either reduced gene expression or no substantial change, with the exception of the neuronal cluster NN#2, which mostly showed increased gene expression. The highest changes in gene expression (> 300 number of differentially expressed genes) were present in macrophages (MM#1, MM#2), neutrophils (NP#1), neurons (NN#2), fibroblasts (FB#1, FB#2,

FB#3, FB#5), Muscle (MC#1), peridermal cells (PD#1, PD#2), as well as in keratinocytes (KC#1, KC#2) and red blood cells (RB#1) (Fig. 4D). This indicates wide-spread changes in gene expression across cell types when *sema4ab* is disrupted.

Since *sema4ab* expression is highly enriched in macrophages (Suppl. Fig. 6D, cf. Fig.1) we analysed macrophage populations in more detail. Interestingly, the two clusters that showed the highest number of differentially expressed genes between control and experimental samples, MM#1 and MM#2, also showed the strongest expression of *sema4ab* (Fig. 4E; Suppl. Fig. 5D). Using *apoeb* and a marker set from adult zebrafish brain (Zambusi *et al*, 2022) we found that MM#1 and MM#2 expressed higher levels of microglial marker genes, compared to MM#3 and MM#4, which expressed more blood-derived macrophage-related genes. Population MM#2, in contrast to population MM#1, expressed proliferation markers, but otherwise marker expression was very similar between the two populations (Fig. 4E). Therefore, MM#2 likely is a proliferative sub-group of microglia and together with population MM#1 represent microglia. High levels of *sema4ab* expression in microglia is consistent with enriched expression of *sema4ab* in microglial cells found in histology (cf. Suppl. Fig. 1E-G). Hence, gene expression changes in macrophage populations correlate positively with the expression levels of *sema4ab* and suggest specific roles of the gene in cells with a microglia marker signature.

To determine which cellular functions might be affected by gene expression changes in microglia-like cells, we used GOstats for KEGG analysis (Falcon & Gentleman, 2007) on clusters MM#1 and MM#2. This indicated

changes in macrophage activation pathways, namely RIG-I-like receptor signalling (Yoneyama *et al*, 2024), Toll-like receptor signalling pathways (Alhamdan *et al*, 2024) and NOD-like receptor signalling (Almeida-da-Silva *et al*, 2023) (Fig. 4F). Most of the indicator genes were under-represented in the sample in which *sema4ab* was disrupted compared to the control sample (20 of 21 genes for RIG-I-pathway, 29 of 32 for Toll-like receptor pathway; 16 of 17 genes for NOD-like receptor signalling; Suppl. Data file 1), suggesting reduced activation of macrophages in the absence of *sema4ab*.

Analysis of the top down-regulated genes in all macrophages confirms this result (Table 1). For example, the most underrepresented gene, *lyz* (7.47-fold down), is related to a pro-inflammatory state (Barros et al., 2015; MacParland et al., 2018). Similarly, *grn1* (6.57-fold down), which is the second-most underrepresented gene after *sema4ab* disruption, is linked to pro-inflammatory state and cytokine production (Horinokita et al., 2019).

Since the activation state of microglial cells is strongly changed, it is likely that their signalling to other regeneration-relevant cell types is altered. To explore changes in potential cell interactions, we used CellChat (Jin *et al*, 2021), which evaluates cell interactions based on known ligand-receptor interactions in scRNAseq data. Indeed, a specific analysis of outgoing interactions from macrophage populations MM#1 and MM#2 showed outgoing interactions with a large number of other cell types. Prominent interactions were found within the macrophage clusters. Most of these interactions were reduced, when *sema4ab* was disrupted (Fig. 4G).

Cell types with altered cell signalling included fibroblasts, which have pivotal functions in successful spinal cord regeneration in zebrafish (Tsata &

Wehner, 2021). We therefore analysed macrophage/fibroblast interactions in more detail. When *sema4ab* was disrupted, outgoing interactions with fibroblast were generally reduced. Affected pathways included cytokine signalling (*e.g. tnfb, tgfb1b)*, among other pathways in CellChat analysis (Suppl. Fig. 5E). In addition, KEGG analysis for the three fibroblast populations that showed highest levels of differentially expressed genes after *sema4ab* disruption (FB#1, FB#2, FB#3) highlighted ECM-receptor interactions, TGF-beta signalling, and adherens junction pathways as changed (Fig. 4H). This data suggests that in general, ECM-related and signalling functions are changed in fibroblasts when *sema4ab* is disrupted. Since fibroblasts show only low levels of *sema4ab* expression themselves, changes in fibroblast gene expression when *sema4ab* is disrupted could be either a direct or indirect consequence of the reduced signalling activity from *sema4ab* expressing macrophages.

Disruption of *sema4ab* does not induce major changes in numbers and behaviours of invading cell types

To characterize the influence of *sema4ab* on the lesion site environment *in situ*, we analysed the numbers of cells invading the lesion site with known roles in regeneration, namely neutrophils, macrophages and fibroblast-like cells (de Sena-Tomas *et al*, 2024; Tsarouchas *et al.*, 2018; Tsata *et al.*, 2021; Wehner *et al.*, 2017) (Suppl. Fig. 6A). The number of neutrophils (*mpx:GFP*+) in the lesion site was unchanged between lesioned control gRNA-injected larvae and *sema4ab* haCR-injected larvae at 4 hpl (peak of neutrophil invasion) and 24 hpl (peak of regenerative neurogenesis) (Suppl. Fig. 6B,C). Macrophages (*mpeg*:*mCherry*+) were moderately reduced in number by 12 % in *sema4ab* haCR injected larvae (Suppl. Fig. 6D) at 24 hpl and the density of fibroblasts

(*pdgfrb:GFP*+) remained unchanged in the absence of *sema4ab* function (Suppl. Fig. 6E). Hence, numbers of crucial cell types that are recruited to the lesion site remained largely unchanged, confirming data from scRNAseq.

To determine whether macrophage behaviour was altered in the absence of *sema4ab*, we analysed phagocytosis of cellular debris, which is one of the major functions of macrophages (Yu *et al*, 2022). We used acridine orange staining to detect levels of cellular debris as a proxy for efferocytosis. The average fluorescence intensity of acridine orange in the lesion site was comparable between control gRNA-injected larvae and *sema4ab* haCR-injected ones at 24 hpl (Suppl. Fig. 6F). Similarly, the number of macrophages with acridine orange-positive inclusions, as indicators of phagocytosed debris, did not show differences in these experimental groups (Suppl. Fig. 6G). This suggests that efferocytosis of debris by macrophages was not grossly altered in *sema4ab*-deficient macrophages.

Cytokine signalling is altered in *sema4ab*-deficient animals

scRNAseq indicated a change in the activation state of *sema4ab* deficient macrophages, which could lead to an altered cytokine milieu in the injury site. Therefore, we analysed expression levels of *serum amyloid A* (*saa*), an inflammation marker and regulator of cytokine release (Song *et al*, 2009), and major pro- (*il1b, tnfa, il6, il11b*) and anti- (*tgfb1a, tgfb3*) inflammatory cytokines and markers in the lesion site environment by qRT-PCR in control gRNA- and *sema4ab* haCR-injected lesioned larvae at 4 and 24 hpl (Fig. 5A) (Woodcock & Morganti-Kossmann, 2013). *il1b*, *tnfa*, and *il6* did not show any changes at 4 hpl (Fig. 5B), when the immune response was dominated by neutrophils. However, reduced expression levels of *il1b* (by 50 %), *tnfa* (by 75

%), and *il6* (by 65 %), together with those of *il11b* (by 45 %) and *saa* (by 75 %), were detected at 24 hpl (Fig. 5C), at the peak of macrophage invasion. At that time point, levels of *tgfb1a* expression were slightly reduced (by 20 %), whereas those of *tgfb3* were more than doubled (120 % increase; Fig. 5D). Overall, qRT-PCR results indicate a shift from a pro-inflammatory to an anti-inflammatory lesion environment in the absence of *sema4ab* function.

To identify possible receptors mediating the effect of Sema4ab on the cytokine environment, we functionally screened additional potential Sema4ab receptors (*havcr1, havcr2, nrp1b, plxnd1*) using haCR disruption and analysis by qRT-PCR, but none of these replicated the pattern of *sema4ab* disruption in reducing expression *il1b*, *tnfa*, *il11b* and *saa,* or increasing expression *of tgfb3* (Suppl. Fig. 7). This suggests more complex interactions of *sema4ab*+ macrophages with cells in the lesion site environment.

To track the cellular sources of the changes in cytokine gene expression observed after *sema4ab* disruption in the lesion site environment, we used transgenic reporter lines and HCR-FISH in histological preparations at 24 hpl (Suppl. Fig. 8A). We found that the number of *il1b:GFP* double-positive macrophages (mpeg:*mCherry*) remained unchanged, but *il1b:GFP* fluorescence intensity was reduced in *sema4ab* haCR-injected larvae, compared to control gRNA-injected larvae (Suppl. Fig. 8B). The number of *tnfa:EGFP*+ macrophages, as well as fluorescence intensity for *tnfa:EGFP* was likewise reduced (Suppl. Fig. 8C). In HCR-FISH we found that *saa* labelling intensity was decreased (Suppl. Fig. 8D). This confirms results from qRT-PCR and indicates changes in cytokine signalling from macrophages after *sema4ab* disruption.

Fibroblasts increase *tgfb3* expression in the absence of *sema4ab* function in macrophages

In HCR-FISH, the labelling intensity of *tgfb3* mRNA was generally increased in *sema4ab haCR* injected animals compared to control gRNA injected controls, in agreement with qRT-PCR results (Suppl. Fig. 9A,B). Remarkably, co-localisation studies indicated that the *tgfb3* signal was not detectable in macrophages (*mpeg*:*mCherry*+). Instead, the signal was present mostly in fibroblasts (*pdgfrb:GFP*+; Fig. 6A-C and Suppl. Fig. 9C). In contrast, *sema4ab* was almost exclusively expressed in immune cells (cf. Fig. 1; Suppl. Fig. 1; Supp. Fig. 9D). Expression of *tgfb3* in fibroblasts, but not in macrophages was also observed in scRNAseq. Indeed, quantifying the HCR-FISH signal by masking the *tgfb3* signal with those for macrophages and fibroblasts in *mfap4:mCherry* and *pdgfrb:GFP* transgenic fish and applying background subtraction (see Material and Methods) indicated that the signal was located in fibroblasts with no detectable signal in macrophages in either control gRNA- or *sema4ab* haCR-injected lesioned larvae. Moreover, the HCR-FISH signal was increased by 20 % in the fibroblasts (Fig. 6D-E). This suggests a scenario, in which macrophages signal to fibroblasts in the lesion site during regeneration. Indeed, live observation of macrophage (*mpeg:mCherry*) and fibroblasts *(pdgfrb:GFP)* from 10 to 25 hpl indicated close physical interactions between these cell types in the injury site, where macrophages move along elongated stationary fibroblasts (Fig. 6F,G and movie in Suppl. data file 2). No obvious differences in these cell behaviours were detectable between control gRNA- and *sema4ab* haCR-injected larvae. These data suggest that

macrophages are in close contact with fibroblasts and that macrophages may attenuate *tgfb3* expression in fibroblasts in the presence of *sema4ab*.

Fibroblasts promote regenerative neurogenesis via Tgfb3

Tgfb3 signalling has been implicated in neuronal regeneration in the zebrafish retina before (Lee et al., 2020). To test its role in regenerative neurogenesis in the zebrafish spinal cord, we disrupted *tgfb3* genetically in somatic mutants and in a temporally conditional way by pharmacologically blocking Tgfb receptors with the small molecule inhibitor SB431542 (Sun *et al*, 2006). Animals injected with *tgfb3* haCRs showed a 45 % reduction in the number of newly generated motor neurons (EdU+/*mnx1:GFP*+) after spinal lesion, compared to control gRNA-injected lesioned larvae at 48 hpl (Fig. 7A-B). Similarly, adding SB431542 to the larvae reduced the number of newly generated motor neurons by 45 %, compared to DMSO treated controls, at 48 hpl (Fig. 7C-D). These observations support a promoting role of *tgfb3* for regenerative neurogenesis.

Disruption of *tgfb3* abolishes the effect of *sema4ab* disruption on lesion-induced neurogenesis

To determine whether control of *tgfb3* expression by Sema4ab signalling could explain at least in part the role of *sema4ab* in attenuating regenerative neurogenesis, we disrupted both genes simultaneously by co-injecting *sema4ab* and *tgfb3* haCRs. Disruption of both genes was effective, as indicated by RFLP for both targets. In these larvae, lesion-induced generation of motor neurons (EdU+/*mnx1:GFP*+) was indistinguishable from that in lesioned control gRNA-injected larvae (Fig. 7E-F). Hence, disruption of *tgfb3* abolished the augmenting

effect of *sema4ab* disruption on regenerative neurogenesis. This suggests that control of *tgfb3* expression in fibroblasts is a major mechanism by which *sema4ab*+ macrophages control lesion-induced neurogenesis.

Potential *sema4ab* signalling in adult zebrafish and mouse spinal cord injury

To estimate whether the regulation patterns observed here could be conserved across species, we analysed expression of relevant genes in published scRNAseq profiles of the lesioned spinal cord of adult zebrafish (Cigliola *et al.*, 2023) and adult mice (Xue *et al*, 2024). In adult zebrafish, we found expression of *plxnb1a* and *plxnb1b* in clusters of *her4.3*+ ERGs. We confirmed this by HCR-FISH in cross sections of adult spinal cord, where we found expression in the ventricular layer (Suppl. Fig. 10A-C). In scRNAseq data, *sema4ab* reads were present in macrophages (*mfap4+*)*. tgfb3* reads were present in fibroblasts (*pgrfrb*+), but not in macrophages (Suppl. Fig. 10A,B). Similarly, in the sample from the lesioned spinal cord of adult mice, we found selective expression of *Sema4a* in macrophages (*Mpeg1*+) and *Plxnb1* selectively in potential ventricular progenitors (*Foxj1*+). *Tgfb3* was expressed in fibroblasts (*Pdgfra*+), but not in macrophages (Suppl. Fig. 11A,B). This indicated that in the injured adult zebrafish and mouse spinal cord, macrophages, fibroblasts and progenitor cells show comparable selective gene expression to what we observe in larval zebrafish. This is consistent with a potentially conserved role of *sema4ab* in spinal cord injury across vertebrates.

***sema4ab* disruption enhances axon regrowth and impairs recovery of swimming function**

We also tested a possible role of *sema4ab* in other modalities of lesion-induced repair, axon regrowth across a spinal lesion site, and recovery of swimming function. To analyse axon regrowth, we assessed the thickness (cross-sectional area) of the neuronal tissue bridge *(tubb5:dsred* line) re-connecting the spinal cord stumps (Wehner *et al.*, 2017) (Suppl. Fig. 12A-B). We observed a 59 % increase in bridge thickness at 48 hpl in lesioned *sema4ab* haCR injected animals, compared to lesioned control gRNA injected animals. This may be an indirect consequence of more newly generated neurons contributing to axon growth or reflect a direct inhibitory role of *sema4ab* on axon growth (Yoneyama *et al.*, 2024).

Functional recovery was assessed by measuring the distance swum after a vibration stimulus. This indicated a 40 % reduction in swim distance in lesioned *sema4ab* germline mutant, compared to lesioned wild type animals (Suppl. Fig. 12C-D). Uninjured germline mutants swam distances that were not different from those of uninjured wild type larvae (Suppl. Fig. 12E-F). These results demonstrates that *sema4ab* is necessary for recovery of swimming function after injury, but not for development. This phenotype may be related to the role of Sema4A in synapse formation (McDermott *et al*, 2018) (see discussion).

In summary, we propose a model by which Sema4ab from macrophages controls neurogenesis directly through Plxnb1a/b on ERGs and indirectly via control of fibroblast-derived Tgfb3 in successful spinal cord regeneration in zebrafish (Fig. 7G). Sema4ab has additional functions in axon regeneration and behavioural recovery.

DISCUSSION

Here we elucidate the complexity of cell cross-talk in a spinal lesion site that leads to regenerative neurogenesis in larval zebrafish. We show that *sema4ab*, mainly expressed by macrophages, influences several cell types. We provide evidence for major functions of *sema4ab* in attenuating regenerative neurogenesis from ERGs via Plxn1a/b receptors likely directly and, by inhibiting Tgfb3 secretion from fibroblasts, indirectly.

Macrophages may signal directly to ERGs to attenuate regenerative neurogenesis. Both signal (*sema4ab*) and receptors (*plxnb1a/b*) were expressed with high selectivity in macrophages and ERGs, respectively, as indicated by HCR-FISH. However, other cell types may also express low levels of these genes, as suggested by scRNAseq. Direct signalling from macrophages to ERGs has been shown for Tnf (Cavone *et al.*, 2021).

Counter-intuitively for a regenerating system, Sema4ab attenuates regenerative neurogenesis. However, it is not infrequent to observe upregulation of inhibiting factors in regeneration. For example, notch signalling is re-activated after spinal injury in adult zebrafish and attenuates neurogenesis there (Dias *et al*, 2012). In a recent functional screen in the regenerating retina of adult zebrafish, 11 out of 100 regeneration-associated genes have been found to promote and 7 genes to attenuate neuronal regeneration (Emmerich *et al*, 2024). Interestingly, when notch signalling is disrupted, limited neurogenesis can be elicited from ependymal cells in the lateral ventricles of mice, but this leads to depletion of the ependymal cells (Carlen *et al*, 2009). Hence, attenuating factors may be needed to keep the balance between progenitor

maintenance and neuronal differentiation in successful regenerative neurogenesis.

How Sema4ab/Plxn1a/b interactions attenuate regenerative neurogenesis remains to be determined. Sema4ab/Plxn*1a/b* could promote stemness or interfere with proliferation and/or inhibit differentiation of spinal ERG progenitors to increase regenerative neurogenesis. In mice, mutating *PlxnB1* and *PlxnB2* together decreased proliferative activity of progenitors and increased their differentiation in the developing cortex, leading to a net effect of reduced neurogenesis (Daviaud *et al.*, 2016). Our re-analysis of mouse scRNAseq data shows that macrophages in a spinal injury site in mice selectively express *Sema4A* and spinal progenitors express *Plxnb1*. Hence, Sema4A could also contribute to inhibition of neurogenesis in the lesioned spinal cord of mice. A relatively stronger Sema4A signal in mice than in zebrafish could tip the balance to inhibition of neurogenesis after spinal injury.

In addition to potential direct signalling to ERGs, *sema4ab* also maintains the activation state of macrophages. KEGG analysis in macrophage clusters highlighted reduced activity of important activation pathways, related to bacterial (Toll-like receptors),viral (RIG-I) response and initiation of the inflammatory response (Alhamdan *et al.*, 2024; Almeida-da-Silva *et al.*, 2023; Yoneyama *et al.*, 2024) to be changed after disruption of *sema4ab* and the top down-regulated genes, including activation markers such as *grn1* (Purrahman *et al*, 2023), confirm this change in activation state. In mammals, macrophages and microglia cells also express Sema4A (Leitner *et al.*, 2015; Meda *et al.*, 2012), including in a spinal lesion site, as analysed here. In agreement with our findings, injecting exogenous Sema4A into the mouse brain increased activation

of microglia there (Chiou *et al*, 2019). Mammalian macrophages also increase *Sema4A* expression when activated by lipopolysaccharides (Meda *et al.*, 2012). Since the activation state of macrophages and microglia affects cytokine signalling (Raziyeva *et al*, 2021), it was not surprising to detect significant changes in the abundance of different cytokines, in particular a reduction of pro-inflammatory ones, in the injury site in the absence of *sema4ab.*

Changes in the cytokine milieu are the likely reason that disruption of *sema4ab* leads to global changes in the injury site environment. In scRNAseq, we could see profound changes in gene expression in many cell types, however, their abundance in the injury site did not change, as indicated by scRNAseq and histology. Even debris endocytosis by macrophages appeared unaltered. Hence, scRNAseq analysis reveals complex signalling interactions in a spinal injury site that depend on macrophage activation. This data presents a resource for further analysis of the complex lesion site environment.

Combining scRNAseq with HCR-FISH, we here demonstrate that *sema4ab* signalling regulates expression of *tgfb3*, a crucial signalling molecule, in fibroblast-like cells. We find *tgfb3* expression only in fibroblasts by HCR-FISH and scRNAseq, and *sema4ab* mostly in macrophages. Hence, changes of *tgfb3* expression after *sema4ab* disruption are most likely a consequence of perturbed macrophage /fibroblast cross-talk. Interestingly, our re-analysis of mouse scRNAseq data shows expression of *Tgfb3* in fibroblasts, but not in macrophages, and *Sema4A* in macrophages, but not in fibroblasts in a spinal injury site, raising the possibility for similar macrophage/fibroblast cross-talk in a non-regenerating system.

How macrophages signal to fibroblasts is unclear. We tried to find evidence for direct involvement of *sema4ab* signalling. However, somatic mutations of a number of potential receptors for *sema4ab* (Alto & Terman, 2017; Rajabinejad *et al.*, 2020), could not replicate *tgfb3* upregulation (*havcr1, havcr2,nrp1b, plxnd1*) or increased neurogenesis (*plxnb2a, plxnb2b*), or were not detectably expressed by HCR-FISH in non-ERG cells (*plxn1a/b*). It is most likely that fibroblasts react to changed levels of pro-inflammatory cytokines in the injury site. For example, responsiveness of fibroblasts to pro-inflammatory cytokines, such as TNF (Osei *et al*, 2020) and IL-1beta (Pilling *et al*, 2015) is well established and CellChat identified potentially altered *tnfb/tnfrsf1a* receptor/ligand signalling between macrophages and fibroblasts in the absence of Sema4ab signalling.

Our data indicate that fibroblast-produced Tgfb3 promotes regenerative neurogenesis. In the adult zebrafish retina, Tgfb3 has been shown to increase pSmad levels in Müller glia, the retinal progenitor cells, and inhibit their injury-induced proliferation (Lee *et al*, 2020). However, there is also evidence for pro-regenerative functions of Tgfb3 in zebrafish retina regeneration, perhaps through indirect effects (Conedera *et al*, 2021; Lenkowski *et al*, 2013; Sharma *et al*, 2020). In mammals, exogenous TGFB3 has been shown to be a mitogen for retinal cells of the developing rat *in vitro* (Anchan & Reh, 1995). This indicates context-dependent functions for Tgfb3 in neural development and regeneration.

Another aspect of macrophage/fibroblast cross-talk that is relevant to successful spinal cord regeneration is the changed expression of ECM-related genes by fibroblasts after *sema4ab* disruption, as indicated by KEGG analysis. This may lead to a more favourable spinal ECM environment and could at least

in part explain increased axon regeneration in *sema4ab* somatic mutants (Kolb *et al.*, 2023; Tsata *et al.*, 2021; Wehner *et al.*, 2017). Indeed, depleting macrophages cells in spinal cord injury in mammals can lead to a more favourable fibrotic response (Zhu *et al*, 2015). However, in another model of depleting blood-derived macrophages, resident microglia were over-activated (Greenhalgh *et al*, 2018), leading to a worse outcome for recovery. This highlights the complexity of macrophage cross-talk with fibroblasts and other cell types in potential therapeutic interventions.

The altered cytokine environment is also likely to contribute to enhanced axonal regrowth in the absence of *sema4ab* function. Tgfb3 promotes axon regrowth after spinal cord injury in larval zebrafish (Keatinge *et al.*, 2021) and the increased axon regrowth after *sema4ab* disruption in our study fits well with the observed increase in *tgfb3* expression. Interestingly, Tgfb3 signalling is associated with scar-free healing in mammalian models by modifying ECM composition (Shah *et al*, 1995; Weng *et al*, 2020). This points to potential Tgfb3-dependent ECM changes that promote axon regrowth. Hence, *tgfb3* is a pro-regenerative factor after spinal injury, expression levels of which are controlled by *sema4ab.*

The reduced levels of *il1b expression* seen here may also be promoting axon regrowth. Increased levels of *il1b* signalling inhibit axon regeneration in an *irf8* mutant zebrafish, and direct targeting of *il1b* expression (Tsarouchas *et al.*, 2018) or reduction by drug treatment that reduces *il1b* expression (Oprişoreanu *et al*, 2023) partially rescues axon regrowth in that mutant. This indicates that lower expression levels of *il1b* may be beneficial for axon growth. On the other hand, we also see reduced expression of *tnfa* after *sema4ab* disruption, which

does not correlate with the observed increase in axon regrowth. *tnfa*-deficient larvae show reduced axon regrowth, identifying *tnfa* as a pro-regenerative factor (Tsarouchas *et al.*, 2018). This again stresses the complexity of signalling cross-talk in a spinal injury site.

It is interesting that the increased axon bridging observed after *sema4ab* disruption did not translate into improved behavioural recovery. A positive correlation between these read-outs has been observed previously in larval (Tsarouchas *et al.*, 2018; Wehner *et al.*, 2017) and adult (Cigliola *et al.*, 2023; Goldshmit *et al.*, 2012; Huang *et al.*, 2021; Mokalled *et al.*, 2016) lesioned zebrafish. A possible explanation for this apparent discrepancy is that *sema4ab* may have a role in re-establishing synapses, such that disruption of *sema4ab* prevents functionally meaningful re-connections. Indeed, the mammalian homolog Sema4A is important for synapse formation (McDermott *et al.*, 2018), as well as other Sema4 family members, such as Sema4D (Raissi *et al*, 2013) and Sema4B (Burkhardt *et al*, 2005). However, in unlesioned larvae we could not detect differences in swimming bahaviour, indicating that *sema4ab* is not essential for developmental synaptogenesis. Hence, increased axon growth may not lead to improved behavioral recovery, if these axons fail to make proper synapses.

We conclude that the macrophage activation state is crucial for the outcome of a spinal injury. The balance of pro- and anti-regenerative signals from multiple cell types determines the regenerative outcome. Single cell -omics approaches are well placed to unravel such complexity. Here we identify macrophage-derived *sema4ab* as a potentially evolutionarily conserved signal in the regulation of the cytokine milieu and as an inhibitor of regeneration of

neurons and axons. Hence, *Sema4a* may present a potential therapeutic target in non-regenerating mammals.

MATERIALS AND METHODS

Animals

All zebrafish lines were raised and kept under standard conditions (Westerfield, 2000). Zebrafish experiments were performed under state of Saxony licenses TVV 36/2021, TVV 45_2018, and holding licenses DD24-5131/364/11, DD24-5131/364/12. For experimental conditions, larvae up to an age of 5 days post-fertilization (dpf) were used of the following lines: wild type (AB); Tg(*mnx1:GFP*)^{ml2tg} , abbreviated as *mnx1:GFP* (Flanagan-Steet *et al*, 2005); Tg(*Xla.Tubb:DsRed*)^{zf1826}, abbreviated as *tubb5:dsred* (Peri & Nusslein-Volhard, 2008); Tg(*her4.1:EGFP*)^{y83Tg}, abbreviated as *her4.1:EGFP*) (Yeo *et al*, 2007); Tg(*mpx:GFP*)^{uwm1}, abbreviated as *mpx:GFP* (Renshaw *et al.*, 2006); Tg(*mpeg1.1:mCherry*)^{gl23}, abbreviated as *mpeg:mCherry* (Ellett *et al.*, 2011); Tg(*pdgfrb:Gal4ff*)^{ncv24}; Tg(*UAS:GFP*), abbreviated as *pdgfrb:GFP* (Ando *et al*, 2016); Tg(*il1b:GFP*)^{sh445}, abbreviated as *il1b:GFP* (Nguyen-Chi *et al*, 2014); and Tg(*tnfa:EGFP*)^{ump5Tg}, abbreviated as *tnfa:EGFP* (Nguyen-Chi *et al*, 2015).

Spinal cord lesion

Lesions of larvae were performed as previously described (Ohnmacht et al., 2016). Briefly, at 3 dpf, zebrafish larvae were deeply anaesthetized in E3 medium (Nüsslein-Volhard & Dahm, 2002) containing 0,02 % of MS-222 (Sigma). Larvae were then transferred to an agarose plate. After removal of excess water, larvae were placed in lateral positions. A transection of the entire spinal cord was made using a 30G syringe needle at the level of the 15th myotome, without injuring the notochord.

Generation of somatic mutants

Somatic mutations were generated mainly following a previous protocol (Keatinge et al., 2021). CRISPR gRNAs were selected using the CRISPRscan website (www.crisprscan.org/gene) webtools. gRNAs were chosen based on the CRISPRScan score (preferentially > 60), and on the availability of a suitable restriction enzyme recognition site (www.snapgene.com) that would be destroyed by the gRNA. Additional criteria were to avoid the first exon and to target functional domains. 1 nL of gRNA mix (1 µl of Tracer (5nM, TRACRRNA05N, Sigma-Aldrich), 1 µl of gRNA (20µM, Sigma-Aldrich), 1 µL of phenol red (P0290, Sigma-Aldrich) and 1 µL of Cas9 (20µM, M0386M, New England Biolabs) was injected into one-cell stage embryos. gRNA efficiency was tested by restriction fragment length polymorphism analysis (RFLP) in a proportion of larvae for each experiment as an internal experimental control (Keatinge et al., 2021). Sequences for gRNAs, primers for RFLPs and RFLPs can be found in Suppl. Table 5 and Suppl. Fig. 13. All experiments conducted with somatic mutants were carried out with a control injected group with a non-targeting gRNA.

Generation of s*ema4ab* germline mutant and *Tg(mfap4:mCherry-CAAX;myl7:mCerulean)* line.

The *sema4ab* mutant stable line was generated by raising somatic mutants as potential founders, as described (Keatinge et al., 2021). The founder selected to generate the stable line carried a 14 bp insertion in exon 6 that generated a frame shift with a premature stop codon. Sequencing primers were the same as for RFLP.

Macrophages selectively express *mfap4 (Walton et al, 2015).* To generate the *Tg(mfap4:mCherry-CAAX;myl7:mCerulean)* line (abbreviated as

mfap4:mCherry), pDEST *mfap4:turquoise2* vector purchased from Addgene (#135218) was used to PCR-amplify the *mfap4* promoter sequence with primers designed to introduce 5´ SacI and 3´ AscI. In parallel, a second plasmid backbone containing *ins:nls-mCerulean; cryaa:mCherry* (previously generated in the group) was digested with SacI/AscI and ligated with mfap4 using SacI/AscI sites *(mfap4:nls-mCerulean; cryaa:mCherry).* Subsequently, mCherry was PCR amplified by using primers designed to introduce 5´ EcoRI and 3´ CAAX box followed by a stop codon and PacI. Then *mfap4:nls-mCerulean; cryaa:mCherry* were digested and ligated using EcoRI/PacI to mCherry-CAAX fragment *(mfap4:mCherry-CAAX; cryaa:mCherry).* Finally, the newly generated *mfap4:mCherry-CAAX; cryaa:mCherry* construct and *ins1.1:ins-sepHLourin; myl7:NLS-mCerulean* construct (previously generated in the lab) were digested with EcoRI/PacI to yield compatible fragments which were ligated together to generate the final construct *(mfap4:mCherry-CAAX;myl7:mCerulean).*The entire construct was flanked with I-Sce sites to facilitate transgenesis and was injected in wild type AB eggs. Several founders were selected based on mCerulean (blue) expression in the heart and mCherry (red) expression in macrophages and the founder with Mendelian segregation in the F1 was selected. Primers are described in Suppl. Table 6.

In situ hybridization chain reaction (HCR-FISH)

Larvae were collected in E3 medium and incubated with 0.003 % 1-phenyl 2-thiourea (PTU) at 6 hpf to suppress melanocyte development. Larvae were fixed overnight in 4 % paraformaldehyde (PFA) at 4 ºC and then transferred to 100 % Methanol (MeOH) at -20 °C overnight for permeabilization. The next day, larvae were rehydrated in a graded series of MeOH at room

temperature (RT) and subsequent washes in phosphate buffered saline with 0.1 % Tween (PBST). Thereafter, larvae were treated with 500 µL proteinase K (Roche) at a concentration of 30 µg/mL for 45 min at RT, followed by post-fixation in 4 % PFA for 20 min RT and washes with PBST (3 x 5 min). Pre-hybridisation was performed using 500 µL of pre-warmed probe hybridisation buffer (Molecular Instruments (Choi et al., 2018)) for 30 min at 37 °C. The probe sets, which were designed based on the NCBI sequence by Molecular Instruments (Choi et al., 2018), were prepared using 2 pmol of each probe set in 500 µL of pre-warmed hybridisation buffer. Then, buffer was replaced with probe sets and incubated for 16 h at 37 °C. On the following day, samples were washed 4 x 15 min with pre-warmed probe washing buffer (Molecular Instruments) at 37 °C followed by 2 x 5 min in 5x sodium chloride sodium citrate with 0.1 % Tween (SSCT) at RT. Larvae were then treated with 500 µL of room temperature equilibrated amplification buffer (Molecular Instruments, LA, USA) for 30 min at RT. Hairpin RNA preparation was performed following the manufacturer's instructions. Samples were incubated with Hairpin RNAs for 16 h in the dark at RT. Finally, samples were washed for 3 x 30 min in 5 x SSCT at RT and immersed in 70 % glycerol for imaging on a Zeiss LSM980 confocal microscope.

For HCR-FISH on adult animal, fish were killed, perfusion-fixed with 4% para-formaldehyde, and tissue slices of 50 µm thickness were obtained from dissected unlesioned spinal cord using a vibrating blade microtome (VT1200S, Leica, Wetzlar, Germany), as described (Becker *et al*, 1997). HCR was performed right away following the protocol described above for larvae, with the

exception that no permeabilization steps were applied (starting directly with hybridization blocking buffer step).

Combining EdU and motor neuron labelling

Labelling newly generated motor neurons followed previous protocols (Ohnmacht et al., 2016). Briefly, lesioned and unlesioned larvae were incubated in E3 medium containing 1 % dimethylsulfoxide (DMSO, Sigma-Aldrich, Taufkirchen, Germany) and 1:100 EdU (Thermo-Fisher, Schwerte, Germany) for 48 h. Samples were fixed in 4 % PFA for 3h at RT and permeabilised in 100 % MeoH at -20 ºC for at least overnight. Larvae were then rehydrated, tails were dissected and incubated in proteinase K (Roche, Sigma-Aldrich) for 45 min at RT at a concentration of 10 µg/mL and then postfixed at RT in 4 % PFA for 15 min. Then, larvae were incubated for 20 min at RT in 0.5 % DMSO-PBST and incubated for 2 h at RT with the Click-it Chemistry Edu Alexa 647 kit (Thermo-Fisher, Waltham, USA) as described by the manufacturer. Subsequently, tails were washed in PBST and incubated with blocking buffer solution (2 %BSA, 1 % DMSO, 1 % Triton, 10 % Normal donkey serum, in PBST) for 1 h at RT and then with a chicken anti-GFP antibody, (1:200, Abcam, Cambridge, UK) at 4 ºC for 48 hours. Secondary antibody (alexa-488 anti-chicken, 1:200, Jackson Immuno) incubation took place overnight at 4 ºC. Finally, samples were washed in PBST and transferred to 70 % glycerol in PBST, mounted and imaged. Imaging was performed using a Widefield Axio Observer (Inverted) with ApoTome 2 Unit (Zeiss). Images were analysed using Fiji (Rueden *et al*, 2017; Schindelin *et al*, 2012). Newly generated motor neurons were counted by assessing the number of double-positive cells for GFP and EdU. Cells were counted manually along the Z-stack, ensuring

counting individual cells in single optical sections, in 50 µm windows located at both sides of the injury site (100 µm in total). Experimental conditions were occluded for the analysis. At least two independent experiments were performed. Individual experiments were merged and analysed for statistical significance.

Generation of Heat shock plasmid and treatment

To create the pTol:sema4ab-T2a-mcherry plasmid, we modified the pTol-hsp70l:mCherry-T2A-atho1b vector (Ezhkova *et al*, 2023). We PCR-amplified the *sema4ab* coding sequence from genomic cDNA and PCR-amplified T2a-mcherry with specific primers (Suppl. Table 7). Then, we performed a simultaneous multiple fragment ligation in the opened backbone vector. The final construct pTol-hsp70l:sema4ab-T2a:mcherry was verified by sequencing, qRT-PCR for over-expression and mCherry fluorescence after injection.

Measurement of axonal regrowth

As an indicator for successful axon regrowth, we determined the extent of continuous labelling of axons across the spinal cord injury site, termed axonal bridging. As a refinement of previous scoring protocols, we here determined the cross-sectional area of the axonal bridge at its narrowest point. Spinal lesion was performed at 3 dpf as described in larvae that were kept into 0.003 % PTU in E3 water from 72 hpf. The *tubb5:dsred* transgenic line was chosen for this experiment, because neuronal cell bodies and axons are labelled by fluorescence in that line. At 2 hpl, larvae were inspected under a fluorescence stereo-microscope and those larvae with incomplete spinal cord transection and those in which the notochord was inadvertently injured (over-lesioned) were

excluded from the experiment. At 48 hpl, larvae were fixed for 1 h in 4 % PFA and afterwards washed 3 x 5 min with PBST. For microscopy, the larvae were mounted in 70 % glycerol in PBST and imaged right away. Images were taken with a Dragonfly Spinning Disk microscope (Andor/Oxford Instruments, Belfast, UK) with a step size of 1 µm with overall 41 slices.

The bridge thickness was determined by calculating the cross-sectional area of the neuronal tissue bridge using a custom script in Fiji (Rueden *et al.*, 2017; Schindelin *et al.*, 2012). Measures were taken at the narrowest point of the axonal bridge, automatically detected by using a maximum projection of the z-stack and a binary segmentation. Measurements of three independent experiments were then merged and analysed for differences by statistical tests.

Analysis of swimming behaviour

The swimming behaviour was assessed using the ZebraBox (View Point, Lyon, France). As above, under- and over-lesioned larvae were excluded from the experiment at 2 hpl. Subsequently, the larvae were individually arranged in 24-well plates, ensuring representation of all groups on each plate, and kept in the incubator at 28 ºC until 48 hpl. Larval movements were automatically tracked during three repetitions of following the same protocol. The protocol included 1 min of rest, a 1 second vibration stimulus (frequency set at 1000 Hz [target power 100]), followed by 59 seconds of no stimulus. The analysis focused on the time-period of 1 minute encompassing the vibration stimulus (including the 1-second stimulus and the subsequent 59 seconds). For each larva, the mean of their swimming distances over the three repeats was computed. Two independent experiments with an average of 30 larvae per condition were performed and the results were merged for statistical analysis.

Quantitative RT-PCR

Following spinal cord lesion of 3 dpf, RNA extraction was performed at 1 dpl using the RNeasy Mini Kit (Qiagen) according to the manufacturer's instructions (50 larvae/condition). The injury site was enriched by cutting away rostral and caudal parts from the larvae at positions approximately 3 somites away from the lesion site in either direction. cDNA was synthesized using the iScript™ cDNA Synthesis Kit (BioRad, cat #. 1708890) according to the manufacturer's instructions. qRT-PCR was performed using the SsoAdvanced Universal SYBR Green Supermix kit (BioRad) according to the manufacturer's instructions and run in triplicates on a LightCycler 480SW instrument (Roche). For gene-specific primers see Suppl. Table 8. Each condition was normalized to a housekeeping gene and the experimental group was compared to controls by normalizing to the control group. At least three individual experiments were run. For statistical analysis using a One-Sample T-test was used.

Immune cell counting in whole-mounted larvae.

Larvae were lesioned at 3 dpf and fixed for 1 h in 4 % PFA at different time points. Larvae were washed in PBST and transferred to glycerol (70 % in PBST), mounted and imaged immediately using a Widefield Axio Observer (Inverted) with an ApoTome 2 Unit. Images were analysed using Fiji with the experimental condition unknown to the observer. A window of 200 µm width and 75 µm height was placed in the centre of the injury site of individual images, right above the notochord. Cells were counted manually inside the window along the Z-stack. At least two individual experiments were carried out and merged.

Acridine Orange labelling

Larvae of the *mpeg:mCherry* line were incubated after a lesion in 1 µg/ml of Acridine Orange (stock solution 10 mg/ml in water) in E3 for 24 h. Then, fish were washed for 3 x 10 min in E3. Larvae were then mounted in 0.5 % agarose in E3 for live imaging on the Dragonfly Spinning Disk microscope (Andor). To estimate total debris, GFP mean intensity was analysed using a 250x100 µm counting window placed in the centre of the injury site. To determine the number of macrophages that ingested debris, cells positive for both mCherry and GFP were counted in the injury site using same window as before.

Fluorescence intensity/area measurements

Images were analysed with Fiji ImageJ (http:// https://imagej.net/ij/). The region of interest was defined as a rectangle of 400 x 100 µm, centred on the injury site and located right above the notochord. Z-stacks were collapsed in sum intensity projections and then background subtraction was performed before analysing the mean intensity with a custom Fiji macro to automatize the process (Rueden *et al.*, 2017; Schindelin *et al.*, 2012). Mean intensity was represented by normalizing each value to the control average value.

Drug treatment of larvae

SB431542 (Fisher Scientific) was dissolved in DMSO to a stock concentration of 10 mM. The working concentration was 50 µM prepared by a dilution of the stock solution in E3. Larvae were pre-treated for 2 h before injury and then incubated for 48 hpl. Control larvae were treated with DMSO at the same concentration.

Cell dissociation and fluorescence-activated sorting

We used 50 larvae per sample. We enriched lesion-site tissue by dissecting 3 somites rostral and caudal of the injury site and collecting them in cold 1 x PBS. The tissue was dissociated using the Miltenyi Neural Tissue Dissociation Kit (P) with addition of collagenase. In brief, we removed excess 1x PBS and added 950 µL Buffer X. We added 6 µL of 1/1000 diluted β-mercaptoethanol, 50 µL Enzyme P and 8 µL collagenase (50 mg/mL). We pipetted the tissue 10 times with 1 mL pipette tips and let it rotate at RT (~22-23 °C) for approximately 1 min. In the meantime, we mixed 10 µL of Buffer Y and 10 µL of Enzyme A and added this to the dissociation mix. We triturated the tissue slowly using fire polished small-orifice glass Pasteur pipette. Each trituration was performed 10 times (6 seconds each time) for 1 min and we let the sample rotate for 1 min. We repeated this step until complete dissociation. We stopped the reaction after ~14 mins by adding 1 mL of DMEM + FBS (1 %) + Protease Inhibitor (1 x) mix (DFP) and performed centrifugation at + 4 °C at 500 g for 5 mins. We removed the supernatant and resuspended the pellet in 1 mL of HBSS (Mg2+/Ca+) + Protease Inhibitor (1x) and then passed it through a 40 µm filter equilibrated with 200 µL of DFP. Cells were recentrifuged at +4 °C at 500 g for 5 mins. The pellet was resuspended in 300 µL of DFP. Just before cell sorting, we added 0.5 µL of propidium iodide (100 µg/mL) and mixed well by pipetting. We sorted viable, propidium iodide-negative cells using FACS Aria (BD Biosciences) using a 100 µm nozzle at flow rate 1. We sorted 100,000 cells per sample in BSA coated 1.5 mL Eppendorf tubes with 500 µL of a 0.4 % BSA solution in 1x PBS. The sorted cells volume was around 200 µL and the final concentration of BSA was 0.28 %. One control gRNA and two *sema4ab* gRNA

samples were processed by the Dresden Concept Genome Center for cell encapsulation using the 10X Genomic V3.

Droplet encapsulation and single-cell RNA sequencing

Cells were pelleted at 500 g for 5 minutes at 4°C, leaving 20 µL of suspension. Cell viability was assessed with trypan blue, and samples with > 80 % viability were prepared for encapsulation. Single-cell RNA sequencing followed the 10x Genomics (Chromium Single-cell Next GEM 3' Library Kit V3.1) workflow (Zheng *et al*, 2017). In brief, cells were mixed with Reverse Transcription Reagent and loaded onto a Chromium Single Cell G Chip, targeting 10,000 cells per sample. GEM generation, barcoding, reverse transcription, cDNA amplification, fragmentation, and purification were performed according to the manufacturer's protocol. Libraries were prepared using 25 % of cDNA, quantified, and sequenced on an Illumina NovaSeq 6000 in 100 bp paired-end mode.

Alignment to zebrafish genome

The raw sequencing data were processed with the 'count' command of the Cell Ranger software (v7.1) provided by 10x Genomics. To build the reference, the zebrafish genome (GRCz11) and gene annotation (Ensembl 109), were downloaded from Ensembl (https://www.ensembl.org/). We used the 'count' command to generate count matrices that were further used by Seurat V5 for downstream analyses.

Quality Control and Doublet Removal

For data analyses, we kept cells based on the following conditions: (i) nFeature_RNA >= 200 (number of genes detected per cell), 500 < nCount_RNA

< 50000 (number of total reads detected per cell), (ii) percent.mt > 20 % (mitochondrial RNA percentage), (iii) nCount_RNA/nFeature_RNA > 20-fold (an indication of possible doublets), (iv) genes found in fewer than 3 cells were removed from the analyses. Additionally, we determined doublets using scDblFinder V1.18.0 (Germain *et al*, 2021). However, we still had rare cells expressing markers for cell types distinct from the clusters they were allocated to, which were possible doublets. We removed these cells, if cells other than neurons expressed *elavl3* or *elavl4*, if cells other than red blood cells expressed *hbbe1.3/hbbe2*, if cells other than muscle, fibroblast-like cells or keratinocytes expressed *col12a1a*, *col12a1b*, or if cells other than muscle or fibroblast-like cells expressed *fgl1,* or *vwde*. Using this method an additional ~5% of cells per sample were removed.

Seurat Data Analyses

After filtering out low-quality cells and doublets, we utilized Seurat V5 for data integration using the CCAIntegration method, following the standard pipeline. A Seurat object was created, and the data were normalized. The top 2,000 variable genes were identified, and the data were scaled using all genes, with nCount_RNA regressed out. Clustering was performed at a resolution of 1.0, yielding 44 distinct clusters (0–43).

After removing low-quality cells and doublets, we utilized Seurat V5 for data integration using CCAIntegration method and followed its standard pipeline. Briefly, a Seurat object was created and the data were normalized. The top 2000 variable genes were identified, and the data were scaled using all genes, with nCount_RNA regressed out. Clustering was performed at resolution 1, yielding 44 distinct clusters (numbered as 0-43).

Finding Marker Genes and annotation of clusters

To identify marker genes (the genes which are specific to a cluster compared to the remaining all other cell types), we used the FindAllMarkers function from Seurat, using the default options. The “Wilcoxon rank sum test”, and p_val_adj (p-value adjusted) < 0.1 and avg_log2FC >= 0.25 (average log2 fold change) was used for selecting significantly expressed marker genes. Additionally, we selected genes using pct.1 (percentage in the cluster) > 0.2 and ordered genes based on their agvg_log2FC in descending order for each cell cluster. Based on the literature, we selected known cell type marker genes from the top ranked genes and annotated the main cell types accordingly.

We annotated the main cell types using the following marker genes and the top-ranked genes for each cluster (Cavone *et al.*, 2021; Chen *et al*, 2023; Farrell *et al*, 2018): Ependymoradial Glia (ERG; *fabp7a, sox2*), Enteric Nervous System (ENS; phox2aa, phox2b), Fibroblast-Like Cells (FBL; 3 main clusters, *col12a1a*, *col12a1b*, *pdgfrb*+), Keratinocytes (KC; *pfn1, krt4*), Peridermis (PD; *krt5, krt91, icn2)*, Muscle Cells (MC; m*eox1, mylz3*), Xanthophores (XP; *gch2, aox5)*, Oligodendrocyte (OD; *cldnk, mbpb, mpz*), Kolmer-Agduhr Cells (KA; *npcc, sst1.1*), neutrophils (NP; *lcp1, mpx, lyz*), macrophages (MM; *lcp1, mfap4, mpeg1.1*), Neurons (NN; *elavl3, elavl4*), Endothelia Cells (EC; *kdrl, cldn5b*), Notochord (NC; s*hha, gas2b*), Red Blood Cells (RBC; *hbbe1.3, hbbe2*) and 5 clusters that remained not annotated (c#28, c#31, c#32, c#34 and c#36).

Differentially Expressed Gene Analysis (DEG)

We used the FindMarkers function in Seurat to determine the differentially expressed genes using “Wilcoxon rank sum test”. We used

p_val_adj < 0.1 and abs(avg log2FC) >= 0.25 for selecting significantly expressed genes.

Gene Ontology term and KEGG Analyses

For KEGG (Kyoto Encyclopedia of Genes and Genomes) analyses we used GOstats (Falcon & Gentleman, 2007) giving all differentially expressed genes (over- or under-represented) using 0.25 log2FC and p_value < 0.05 as input. We selected enriched terms with a p-value < 0.05.

Cell-Cell Interaction

We used CellChat V2.1.0 (Jin *et al.*, 2021) for cell-cell interaction and a custom cell-cell interaction as described (Cosacak et al. 2019). In brief, we modified the CellChat Database by adding *sema4ab* as ligand and *plxnb1a, plxnb1b, plxnb2a, plxnb2b, plxnd1, havcr1, havcr2, nrp1a and nrp1b* as its receptors. As there was a pathway named SEMA4, we renamed the pathway to “SEMA4AB” for *sema4ab* and to “SEMA4other” for *sema4c/sema4g*. Then, we created CellChat objects for each data set using normalized data from the integrated Seurat object. Finally, the CellChat objects were merged for comparative analyses.

Time-lapse microscopy

Zebrafish larvae were prepared for time lapse microscopy based on our established protocol (https://ibidi.com/img/cms/support/UP/UP12_Zebrafish_Co_Culture.pdf). Briefly, double transgenic zebrafish larvae (*pdgfrb:GFP*; *mfap4:mCherry*) were lesioned at 3 dpf and anaesthetized with MS-222 (160 mg/L in E3 medium). Low melting point agarose (0.5 %, Biozym Plaque Agarose - Low melting Agarose #840100)

was prepared in E3 medium and allowed to cool down to 38 °C before adding MS-222 (final concentration 80 mg/L). Anaesthetized zebrafish larvae were transferred to the agarose and one by one positioned into individual wells of the chambered coverslip. Six larvae were used in total; three control gRNA-injected and three *sema4ab* haCR-injected ones. Microscopy was performed with a Dragonfly Spinning Disk microscope (Andor/Oxford Instruments, Belfast, UK) with a temperature-controlled stage at 28 °C using a 20x objective (20x/0.75 U Plan SApo, Air, DIC, OLYMPUS, Tokyo, Japan). The GFP fluorophore was excited with a 488 nm laser (laser power 20 %) with an exposure time of 180 ms and the mCherry flourophore was excited with a 561 nm laser (laser power 50 %) with an exposure time of 900 ms. We acquired z-stacks of 43 optical sections, with a step size of 1 µm. The interval between single frames of the time-lapse movies was 6 minutes. Time-lapse was performed from 10 hpl until 25 hpl.

Bias mitigation and statistical analysis

The experimental conditions were occluded before manual counting and analysis and processing was automated where possible (e. g. measurements of axonal regrowth and intensity measurements). For manual counts of EdU+ cells, pilot experiments were performed by two independent experimenters, both showing comparable effect sizes. Experiments were performed in duplicate, if not indicated differently.

Statistical methods to analyse scRNAseq data are described above. For all other experiments, quantitative data was tested for normality using Shapiro-Wilk's W-test. Then, parametric (unpaired Student's t-test or one-way ANOVA) and non-parametric (Mann-Whitney U test or Kruskal-Wallis test) were applied

as appropriate. Error bars in figures indicate standard error of the mean (SEM), p-values were represented as asterisks in the figures (*$p < 0.05$; **$p < 0.01$; *** $p < 0.001$) and exact p-values are given in figure legends. To generate graphs and for statistical analysis we used GraphPad Prism 8 (GraphPad Software, Boston, USA).

Figure preparation

Images were adjusted for brightness, contrast and intensity. Drawings were made using CorelDraw X8 (Corel/Alludo, Ottawa, Canada). Figure plates were prepared using CorelDraw X8 (Corel/Alludo, Ottawa, Canada) and Adobe Photoshop 2024 (Adobe, CA, USA).

Data availability

The scRNA-seq raw data of zebrafish larvae generated in this study can be accessed at NCBI GEO accession no. xx. Additional datasets used in this are publicly accessible at NCBI GEO accession numbers; GSE213435 (adult zebrafish spinal cord injury), GSE218584 (mouse data). The R-source codes for single-cell analyses are available on GitHub; https://github.com/micosacak/scRNA_seq_zebrafish_sema4ab.

ACKNOWLEDGEMENTS

We thank Dr. Stefan Hans for reagents; Drs Hella Hartmann and Ruth Hans for imaging advice; Dr. Daniel Wehner for critical reading; and Dr. Judith Konantz, Marika Fischer, and Silvio Kunadt for fish care. This work was supported by the Light Microscopy Facility, the DRESDEN-concept Genome Center, the Flow Cytometry Facility, and the Zebrafish Facility, all core facilities of the Center for Molecular and Cellular Bioengeneering (CMCB) at the Technische Universität (TU) Dresden. Funding was provided by the BBSRC (BB/T015594/1 to TB, CGB), an Alexander von Humboldt Stiftung Professorship award (to CGB), and TU Dresden core funding (to CGB).

AUTHOR CONTRIBUTIONS (CRediT nomenclature)

ADS: conceptualization, methodology, validation, formal analysis, investigation, writing - original draft, writing - review and editing, visualisation, supervision; MIC: methodology, validation, formal analysis, investigation, writing - review and editing; KH: methodology, validation, formal analysis, investigation, visualization; FK: software; methodology; AMO: investigation; ÖC: investigation, DZ: investigation; JA: investigation, AB: investigation; formal analysis; AH: resources; NN: resources; CGB: conceptualization, writing - original draft, writing - review and editing, visualisation, supervision, funding acquisition; TB: conceptualization, writing - original draft, writing - review and editing, visualisation, supervision, funding acquisition.

REFERENCES

Alhamdan F, Bayarsaikhan G, Yuki K (2024) Toll-like receptors and integrins crosstalk. *Front Immunol* 15: 1403764

Almeida-da-Silva CLC, Savio LEB, Coutinho-Silva R, Ojcius DM (2023) The role of NOD-like receptors in innate immunity. *Front Immunol* 14: 1122586

Alto LT, Terman JR (2017) Semaphorins and their Signaling Mechanisms. *Methods in molecular biology (Clifton, NJ)* 1493: 1-25

Anchan RM, Reh TA (1995) Transforming growth factor-beta-3 is mitogenic for rat retinal progenitor cells in vitro. *J Neurobiol* 28: 133-145

Ando K, Fukuhara S, Izumi N, Nakajima H, Fukui H, Kelsh RN, Mochizuki N (2016) Clarification of mural cell coverage of vascular endothelial cells by live imaging of zebrafish. *Development* 143: 1328-1339

Becker CG, Becker T (2015) Neuronal regeneration from ependymo-radial glial cells: cook, little pot, cook! *Dev Cell* 32: 516-527

Becker CG, Lieberoth BC, Morellini F, Feldner J, Becker T, Schachner M (2004) L1.1 is involved in spinal cord regeneration in adult zebrafish. *J Neurosci* 24: 7837-7842

Becker T, Wullimann MF, Becker CG, Bernhardt RR, Schachner M (1997) Axonal regrowth after spinal cord transection in adult zebrafish. *J Comp Neurol* 377: 577-595

Briona LK, Dorsky RI (2014) Radial glial progenitors repair the zebrafish spinal cord following transection. *Exp Neurol* 256: 81-92

Briona LK, Poulain FE, Mosimann C, Dorsky RI (2015) Wnt/beta-catenin signaling is required for radial glial neurogenesis following spinal cord injury. *Dev Biol* 403: 15-21

Burkhardt C, Muller M, Badde A, Garner CC, Gundelfinger ED, Puschel AW (2005) Semaphorin 4B interacts with the post-synaptic density protein PSD-95/SAP90 and is recruited to synapses through a C-terminal PDZ-binding motif. *FEBS Lett* 579: 3821-3828

Carlen M, Meletis K, Goritz C, Darsalia V, Evergren E, Tanigaki K, Amendola M, Barnabe-Heider F, Yeung MS, Naldini L *et al* (2009) Forebrain ependymal cells are Notch-dependent and generate neuroblasts and astrocytes after stroke. *Nat Neurosci* 12: 259-267

Carvalheiro T, Affandi AJ, Malvar-Fernandez B, Dullemond I, Cossu M, Ottria A, Mertens JS, Giovannone B, Bonte-Mineur F, Kok MR *et al* (2019) Induction of Inflammation and Fibrosis by Semaphorin 4A in Systemic Sclerosis. *Arthritis Rheumatol* 71: 1711-1722

Cavone L, McCann T, Drake LK, Aguzzi EA, Oprişoreanu AM, Pedersen E, Sandi S, Selvarajah J, Tsarouchas TM, Wehner D *et al* (2021) A unique macrophage subpopulation signals directly to progenitor cells to promote regenerative neurogenesis in the zebrafish spinal cord. *Dev Cell* 56: 1617-1630.e1616

Chang W, Pedroni A, Bertuzzi M, Kizil C, Simon A, Ampatzis K (2021) Locomotion dependent neuron-glia interactions control neurogenesis and regeneration in the adult zebrafish spinal cord. *Nat Commun* 12: 4857

Chen F, Kohler M, Cucun G, Takamiya M, Kizil C, Cosacak MI, Rastegar S (2023) sox1a:eGFP transgenic line and single-cell transcriptomics reveal the origin of zebrafish intraspinal serotonergic neurons. *iScience* 26: 107342

Chiou B, Neely E, Kallianpur A, Connor JR (2019) Semaphorin4A causes loss of mature oligodendrocytes and demyelination in vivo. *J Neuroinflammation* 16: 28

Cigliola V, Shoffner A, Lee N, Ou J, Gonzalez TJ, Hoque J, Becker CJ, Han Y, Shen G, Faw TD *et al* (2023) Spinal cord repair is modulated by the neurogenic factor Hb-egf under direction of a regeneration-associated enhancer. *Nat Commun* 14: 4857

Conedera FM, Quintela Pousa AM, Presby DM, Mercader N, Enzmann V, Tschopp M (2021) Diverse Signaling by TGFβ Isoforms in Response to Focal Injury is Associated with Either Retinal Regeneration or Reactive Gliosis. *Cell Mol Neurobiol* 41: 43-62

Daviaud N, Chen K, Huang Y, Friedel RH, Zou H (2016) Impaired cortical neurogenesis in plexin-B1 and -B2 double deletion mutant. *Dev Neurobiol* 76: 882-899

de Sena-Tomas C, Rebola Lameira L, Rebocho da Costa M, Naique Taborda P, Laborde A, Orger M, de Oliveira S, Saude L (2024) Neutrophil immune profile guides spinal cord regeneration in zebrafish. *Brain Behav Immun* 120: 514-531

Dias TB, Yang YJ, Ogai K, Becker T, Becker CG (2012) Notch signaling controls generation of motor neurons in the lesioned spinal cord of adult zebrafish. *J Neurosci* 32: 3245-3252

Dusart I, Schwab ME (1994) Secondary cell death and the inflammatory reaction after dorsal hemisection of the rat spinal cord. *Eur J Neurosci* 6: 712-724

Ellett F, Pase L, Hayman JW, Andrianopoulos A, Lieschke GJ (2011) mpeg1 promoter transgenes direct macrophage-lineage expression in zebrafish. *Blood* 117: e49-56

Emmerich K, Hageter J, Hoang T, Lyu P, Sharrock AV, Ceisel A, Thierer J, Chunawala Z, Nimmagadda S, Palazzo I *et al* (2024) A large-scale CRISPR screen reveals context-specific genetic regulation of retinal ganglion cell regeneration. *Development* 151

Ezhkova D, Schwarzer S, Spiess S, Geffarth M, Machate A, Zoller D, Stucke J, Alexopoulou D, Lesche M, Dahl A *et al* (2023) Transcriptome analysis reveals an Atoh1b-dependent gene set downstream of Dlx3b/4b during early inner ear development in zebrafish. *Biol Open* 12

Falcon S, Gentleman R (2007) Using GOstats to test gene lists for GO term association. *Bioinformatics* 23: 257-258

Farrell JA, Wang Y, Riesenfeld SJ, Shekhar K, Regev A, Schier AF (2018) Single-cell reconstruction of developmental trajectories during zebrafish embryogenesis. *Science* 360

Flanagan-Steet H, Fox MA, Meyer D, Sanes JR (2005) Neuromuscular synapses can form in vivo by incorporation of initially aneural postsynaptic specializations. *Development* 132: 4471-4481

Germain PL, Lun A, Garcia Meixide C, Macnair W, Robinson MD (2021) Doublet identification in single-cell sequencing data using scDblFinder. *F1000Research* 10: 979

Goldshmit Y, Sztal TE, Jusuf PR, Hall TE, Nguyen-Chi M, Currie PD (2012) Fgf-dependent glial cell bridges facilitate spinal cord regeneration in zebrafish. *J Neurosci* 32: 7477-7492

Greenhalgh AD, Zarruk JG, Healy LM, Baskar Jesudasan SJ, Jhelum P, Salmon CK, Formanek A, Russo MV, Antel JP, McGavern DB *et al* (2018) Peripherally derived macrophages modulate microglial function to reduce inflammation after CNS injury. *PLoS Biol* 16: e2005264

Huang CX, Zhao Y, Mao J, Wang Z, Xu L, Cheng J, Guan NN, Song J (2021) An injury-induced serotonergic neuron subpopulation contributes to axon regrowth and function restoration after spinal cord injury in zebrafish. *Nat Commun* 12: 7093

Jin S, Guerrero-Juarez CF, Zhang L, Chang I, Ramos R, Kuan CH, Myung P, Plikus MV, Nie Q (2021) Inference and analysis of cell-cell communication using CellChat. *Nat Commun* 12: 1088

Keatinge M, Tsarouchas TM, Munir T, Porter NJ, Larraz J, Gianni D, Tsai HH, Becker CG, Lyons DA, Becker T (2021) CRISPR gRNA phenotypic screening in zebrafish reveals pro-regenerative genes in spinal cord injury. *PLoS Genet* 17: e1009515

Kolb J, Tsata V, John N, Kim K, Mockel C, Rosso G, Kurbel V, Parmar A, Sharma G, Karandasheva K *et al* (2023) Small leucine-rich proteoglycans inhibit CNS regeneration by modifying the structural and mechanical properties of the lesion environment. *Nat Commun* 14: 6814

Kyritsis N, Kizil C, Zocher S, Kroehne V, Kaslin J, Freudenreich D, Iltzsche A, Brand M (2012) Acute inflammation initiates the regenerative response in the adult zebrafish brain. *Science* 338: 1353-1356

Lee MS, Wan J, Goldman D (2020) Tgfb3 collaborates with PP2A and notch signaling pathways to inhibit retina regeneration. *eLife* 9

Leitner DF, Todorich B, Zhang X, Connor JR (2015) Semaphorin4A Is Cytotoxic to Oligodendrocytes and Is Elevated in Microglia and Multiple Sclerosis. *ASN Neuro* 7

Lenkowski JR, Qin Z, Sifuentes CJ, Thummel R, Soto CM, Moens CB, Raymond PA (2013) Retinal regeneration in adult zebrafish requires regulation of TGFbeta signaling. *Glia* 61: 1687-1697

Liu XZ, Xu XM, Hu R, Du C, Zhang SX, McDonald JW, Dong HX, Wu YJ, Fan GS, Jacquin MF *et al* (1997) Neuronal and glial apoptosis after traumatic spinal cord injury. *J Neurosci* 17: 5395-5406

Llorens-Bobadilla E, Chell JM, Le Merre P, Wu Y, Zamboni M, Bergenstråhle J, Stenudd M, Sopova E, Lundeberg J, Shupliakov O *et al* (2020) A latent lineage potential in resident neural stem cells enables spinal cord repair. *Science* 370: DOI: 10.1126/science.abb8795

McDermott JE, Goldblatt D, Paradis S (2018) Class 4 Semaphorins and Plexin-B receptors regulate GABAergic and glutamatergic synapse development in the mammalian hippocampus. *Mol Cell Neurosci* 92: 50-66

Meda C, Molla F, De Pizzol M, Regano D, Maione F, Capano S, Locati M, Mantovani A, Latini R, Bussolino F *et al* (2012) Semaphorin 4A exerts a proangiogenic effect by enhancing vascular endothelial growth factor-A expression in macrophages. *J Immunol* 188: 4081-4092

Mokalled MH, Patra C, Dickson AL, Endo T, Stainier DY, Poss KD (2016) Injury-induced ctgfa directs glial bridging and spinal cord regeneration in zebrafish. *Science* 354: 630-634

Nguyen-Chi M, Laplace-Builhe B, Travnickova J, Luz-Crawford P, Tejedor G, Phan QT, Duroux-Richard I, Levraud JP, Kissa K, Lutfalla G *et al* (2015) Identification of polarized macrophage subsets in zebrafish. *eLife* 4: e07288

Nguyen-Chi M, Phan QT, Gonzalez C, Dubremetz JF, Levraud JP, Lutfalla G (2014) Transient infection of the zebrafish notochord with E. coli induces chronic inflammation. *Dis Model Mech* 7: 871-882

Nüsslein-Volhard C, Dahm R (2002) *Zebrafish: a practical approach*. Oxford University Press, Oxford, UK

Ohnmacht J, Yang Y, Maurer GW, Barreiro-Iglesias A, Tsarouchas TM, Wehner D, Sieger D, Becker CG, Becker T (2016) Spinal motor neurons are regenerated after mechanical lesion and genetic ablation in larval zebrafish. *Development* 143: 1464-1474

Oprişoreanu AM, Ryan F, Richmond C, Dzekhtsiarova Y, Carragher NO, Becker T, David S, Becker CG (2023) Drug screening in zebrafish larvae reveals inflammation-related modulators of secondary damage after spinal cord injury in mice. *Theranostics* https://www.thno.org/v13p2531

Osei ET, L BM-G, Hsieh A, Warner SM, Al-Fouadi M, Wang M, Cole DJ, Maksym GN, T SH, Timens W *et al* (2020) Epithelial-interleukin-1 inhibits collagen formation by airway fibroblasts: Implications for asthma. *Sci Rep* 10: 8721

Peri F, Nusslein-Volhard C (2008) Live imaging of neuronal degradation by microglia reveals a role for v0-ATPase a1 in phagosomal fusion in vivo. *Cell* 133: 916-927

Pilling D, Vakil V, Cox N, Gomer RH (2015) TNF-alpha-stimulated fibroblasts secrete lumican to promote fibrocyte differentiation. *Proc Natl Acad Sci U S A* 112: 11929-11934

Purrahman D, Shojaeian A, Poniatowski LA, Piechowski-Jozwiak B, Mahmoudian-Sani MR (2023) The Role of Progranulin (PGRN) in the Pathogenesis of Ischemic Stroke. *Cell Mol Neurobiol* 43: 3435-3447

Raissi AJ, Staudenmaier EK, David S, Hu L, Paradis S (2013) Sema4D localizes to synapses and regulates GABAergic synapse development as a membrane-bound molecule in the mammalian hippocampus. *Mol Cell Neurosci* 57: 23-32

Rajabinejad M, Asadi G, Ranjbar S, Afshar Hezarkhani L, Salari F, Gorgin Karaji A, Rezaiemanesh A (2020) Semaphorin 4A, 4C, and 4D: Function comparison in the autoimmunity, allergy, and cancer. *Gene* 746: 144637

Raziyeva K, Kim Y, Zharkinbekov Z, Kassymbek K, Jimi S, Saparov A (2021) Immunology of Acute and Chronic Wound Healing. *Biomolecules* 11

Reimer MM, Sorensen I, Kuscha V, Frank RE, Liu C, Becker CG, Becker T (2008) Motor neuron regeneration in adult zebrafish. *J Neurosci* 28: 8510-8516

Renshaw SA, Loynes CA, Trushell DM, Elworthy S, Ingham PW, Whyte MK (2006) A transgenic zebrafish model of neutrophilic inflammation. *Blood* 108: 3976-3978

Rueden CT, Schindelin J, Hiner MC, DeZonia BE, Walter AE, Arena ET, Eliceiri KW (2017) ImageJ2: ImageJ for the next generation of scientific image data. *BMC Bioinformatics* 18: 529

Schindelin J, Arganda-Carreras I, Frise E, Kaynig V, Longair M, Pietzsch T, Preibisch S, Rueden C, Saalfeld S, Schmid B *et al* (2012) Fiji: an open-source platform for biological-image analysis. *Nat Methods* 9: 676-682

Shah M, Foreman DM, Ferguson MW (1995) Neutralisation of TGF-beta 1 and TGF-beta 2 or exogenous addition of TGF-beta 3 to cutaneous rat wounds reduces scarring. *J Cell Sci* 108 (Pt 3): 985-1002

Sharma P, Gupta S, Chaudhary M, Mitra S, Chawla B, Khursheed MA, Saran NK, Ramachandran R (2020) Biphasic Role of Tgf-β Signaling during Müller Glia Reprogramming and Retinal Regeneration in Zebrafish. *iScience* 23: 100817

Shihabuddin LS, Horner PJ, Ray J, Gage FH (2000) Adult spinal cord stem cells generate neurons after transplantation in the adult dentate gyrus. *J Neurosci* 20: 8727-8735

Song C, Hsu K, Yamen E, Yan W, Fock J, Witting PK, Geczy CL, Freedman SB (2009) Serum amyloid A induction of cytokines in monocytes/macrophages and lymphocytes. *Atherosclerosis* 207: 374-383

Stenudd M, Sabelström H, Llorens-Bobadilla E, Zamboni M, Blom H, Brismar H, Zhang S, Basak O, Clevers H, Göritz C *et al* (2022) Identification of a discrete subpopulation of spinal cord ependymal cells with neural stem cell properties. *Cell Rep* 38: 110440

Sun H, Kawahara Y, Ito K, Kanazawa I, Kwak S (2006) Slow and selective death of spinal motor neurons in vivo by intrathecal infusion of kainic acid:

implications for AMPA receptor-mediated excitotoxicity in ALS. *J Neurochem* 98: 782-791

Sun T, Yang L, Kaur H, Pestel J, Looso M, Nolte H, Krasel C, Heil D, Krishnan RK, Santoni MJ *et al* (2017) A reverse signaling pathway downstream of Sema4A controls cell migration via Scrib. *J Cell Biol* 216: 199-215

Toyofuku T, Nojima S, Ishikawa T, Takamatsu H, Tsujimura T, Uemura A, Matsuda J, Seki T, Kumanogoh A (2012) Endosomal sorting by Semaphorin 4A in retinal pigment epithelium supports photoreceptor survival. *Genes Dev* 26: 816-829

Tsarouchas TM, Wehner D, Cavone L, Munir T, Keatinge M, Lambertus M, Underhill A, Barrett T, Kassapis E, Ogryzko N *et al* (2018) Dynamic control of proinflammatory cytokines Il-1β and Tnf-α by macrophages in zebrafish spinal cord regeneration. *Nat Commun* 9: 4670

Tsata V, Möllmert S, Schweitzer C, Kolb J, Möckel C, Böhm B, Rosso G, Lange C, Lesche M, Hammer J *et al* (2021) A switch in pdgfrb(+) cell-derived ECM composition prevents inhibitory scarring and promotes axon regeneration in the zebrafish spinal cord. *Dev Cell* 56: 509-524.e509

Tsata V, Wehner D (2021) Know How to Regrow-Axon Regeneration in the Zebrafish Spinal Cord. *Cells* 10

Vandestadt C, Vanwalleghem GC, Khabooshan MA, Douek AM, Castillo HA, Li M, Schulze K, Don E, Stamatis SA, Ratnadiwakara M *et al* (2021) RNA-induced inflammation and migration of precursor neurons initiates neuronal circuit regeneration in zebrafish. *Dev Cell* 56: 2364-2380.e2368

Walton EM, Cronan MR, Beerman RW, Tobin DM (2015) The Macrophage-Specific Promoter mfap4 Allows Live, Long-Term Analysis of Macrophage Behavior during Mycobacterial Infection in Zebrafish. *PLoS One* 10: e0138949

Wehner D, Tsarouchas TM, Michael A, Haase C, Weidinger G, Reimer MM, Becker T, Becker CG (2017) Wnt signaling controls pro-regenerative Collagen XII in functional spinal cord regeneration in zebrafish. *Nat Commun* 8: 126

Weng L, Funderburgh JL, Khandaker I, Geary ML, Yang T, Basu R, Funderburgh ML, Du Y, Yam GH (2020) The anti-scarring effect of corneal stromal stem cell therapy is mediated by transforming growth factor beta3. *Eye Vis (Lond)* 7: 52

Westerfield M (2000) *The zebrafish book: a guide for the laboratory use of zebrafish (Danio rerio)*. University of Oregon Press, Eugene

Woodcock T, Morganti-Kossmann MC (2013) The role of markers of inflammation in traumatic brain injury. *Front Neurol* 4: 18

Xue X, Wu X, Fan Y, Han S, Zhang H, Sun Y, Yin Y, Yin M, Chen B, Sun Z *et al* (2024) Heterogeneous fibroblasts contribute to fibrotic scar formation after spinal cord injury in mice and monkeys. *Nat Commun* 15: 6321

Yeo SY, Kim M, Kim HS, Huh TL, Chitnis AB (2007) Fluorescent protein expression driven by her4 regulatory elements reveals the spatiotemporal

pattern of Notch signaling in the nervous system of zebrafish embryos. *Dev Biol* 301: 555-567

Yoneyama M, Kato H, Fujita T (2024) Physiological functions of RIG-I-like receptors. *Immunity* 57: 731-751

Yu F, Wang Y, Stetler AR, Leak RK, Hu X, Chen J (2022) Phagocytic microglia and macrophages in brain injury and repair. *CNS Neurosci Ther* 28: 1279-1293

Zambusi A, Novoselc KT, Hutten S, Kalpazidou S, Koupourtidou C, Schieweck R, Aschenbroich S, Silva L, Yazgili AS, van Bebber F *et al* (2022) TDP-43 condensates and lipid droplets regulate the reactivity of microglia and regeneration after traumatic brain injury. *Nat Neurosci* 25: 1608-1625

Zheng GX, Terry JM, Belgrader P, Ryvkin P, Bent ZW, Wilson R, Ziraldo SB, Wheeler TD, McDermott GP, Zhu J *et al* (2017) Massively parallel digital transcriptional profiling of single cells. *Nat Commun* 8: 14049

Zhu Y, Soderblom C, Krishnan V, Ashbaugh J, Bethea JR, Lee JK (2015) Hematogenous macrophage depletion reduces the fibrotic scar and increases axonal growth after spinal cord injury. *Neurobiol Dis* 74: 114-125

FIGURES

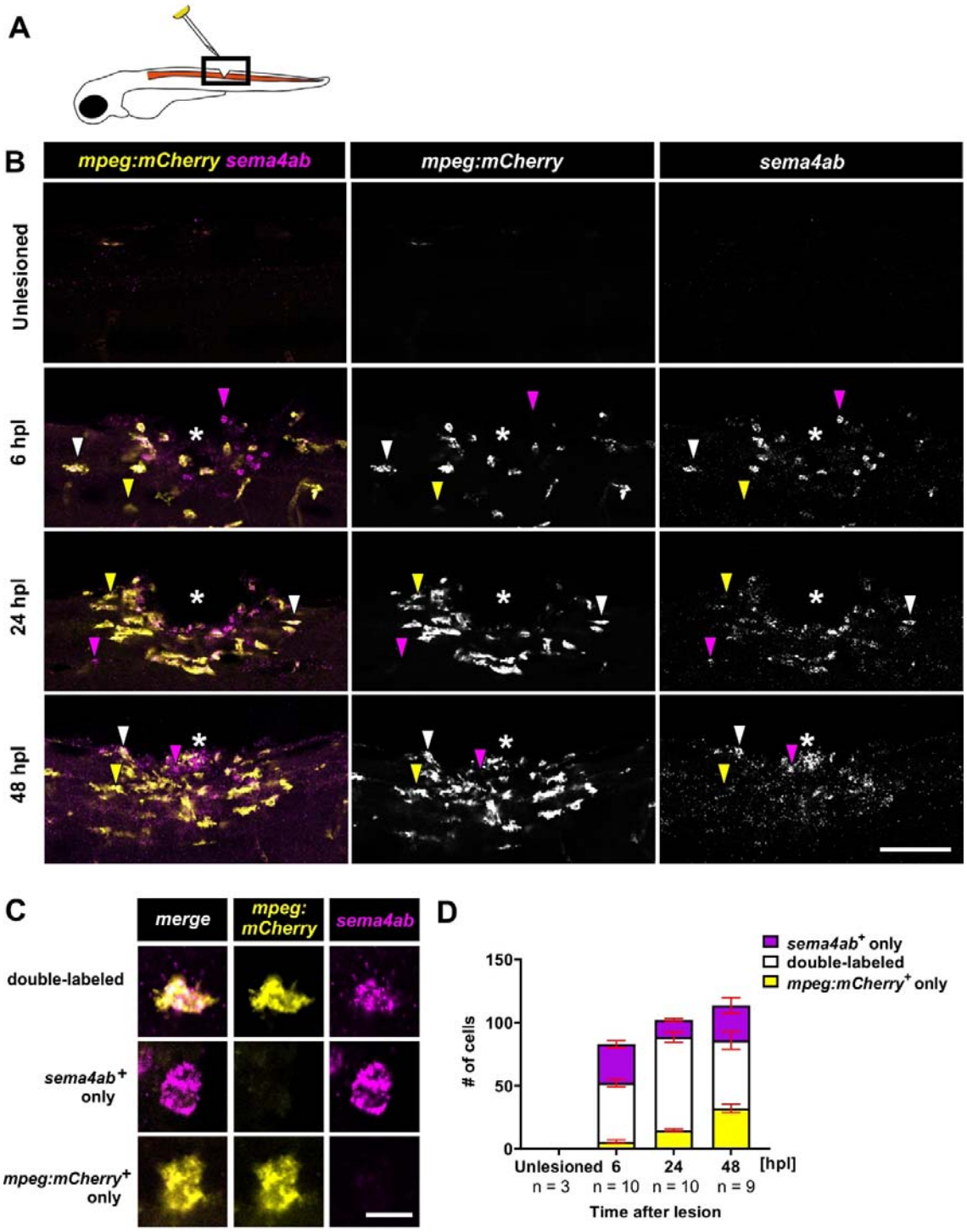
A
B
mpeg:mCherry sema4ab
mpeg:mCherry
sema4ab
Unlesioned
6 hpl
24 hpl
48 hpl
C
merge
mpeg: mCherry
sema4ab
double-labeled
sema4ab+ only
mpeg:mCherry+ only
D
sema4ab+ only
double-labeled
mpeg:mCherry+ only
# of cells
150
100
50
0
Unlesioned
6
24
48
[hpl]
n = 3
n = 10
n = 10
n = 9
Time after lesion

Fig.1. *Sema4ab* is expressed mainly in macrophages in a spinal injury site. (A) Schematic of a zebrafish larva indicating the lateral view of the spinal injury site shown throughout the article, unless specified differently. **(B)** A time-course analysis of multiplexed HCR-FISH indicates extensive overlap of *mpeg*:*mCherry* and *sema4ab* signals during spinal cord repair (white arrows: double positive cells; yellow arrows: *mpeg:mCherry*+ only; magenta arrows: *sema4ab*+ only). **(C)** High magnifications of *mpeg:mCherry/sema4ab* double and single positive cells used for cell counting are shown. **(D)** A quantification of *mpeg:mCherry* and *sema4ab* signal overlap is shown. Error bars show SEM. Asterisks indicate the injury site. Scale bars: 100 µm (B), 10 µm (C).

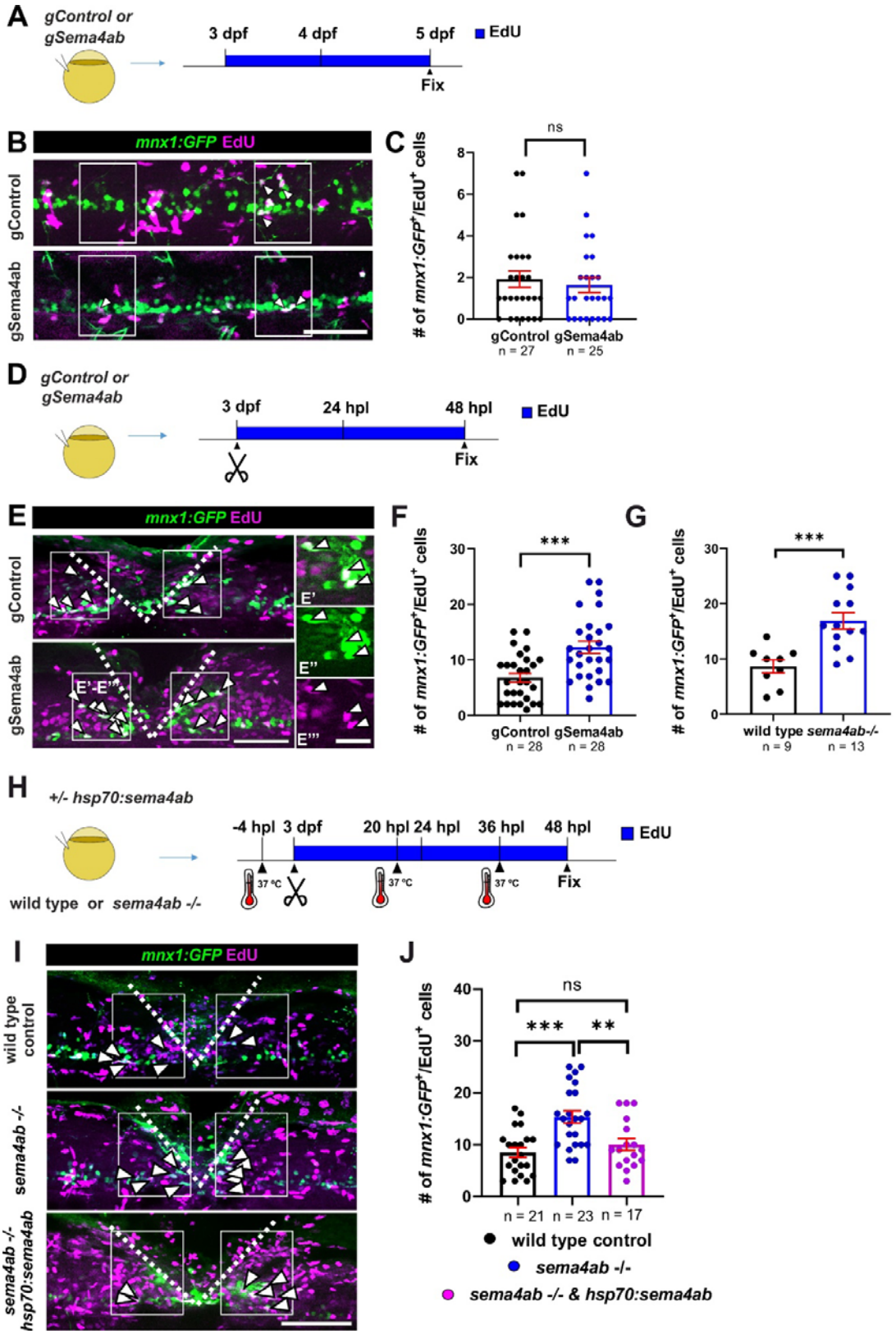
A
gControl or gSema4ab
3 dpf
4 dpf
5 dpf
EdU
Fix
B
mnx1:GFP EdU
gControl
gSema4ab
C
ns
# of mnx1:GFP+/EdU+ cells
gControl
gSema4ab
n = 27
n = 25
D
gControl or gSema4ab
3 dpf
24 hpl
48 hpl
EdU
Fix
E
mnx1:GFP EdU
gControl
gSema4ab
E'-E'''
E'
E''
E'''
F
***
# of mnx1:GFP+/EdU+ cells
gControl
gSema4ab
n = 28
n = 28
G
***
# of mnx1:GFP+/EdU+ cells
wild type
sema4ab-/-
n = 9
n = 13
H
+/- hsp70:sema4ab
wild type or sema4ab -/-
-4 hpl
3 dpf
20 hpl
24 hpl
36 hpl
48 hpl
EdU
37 °C
Fix
I
mnx1:GFP EdU
wild type control
sema4ab -/-
sema4ab -/- hsp70:sema4ab
J
ns
***
**
# of mnx1:GFP+/EdU+ cells
n = 21
n = 23
n = 17
wild type control
sema4ab -/-
sema4ab -/- & hsp70:sema4ab

Fig. 2. *Sema4ab* loss of function increases regenerative neurogenesis. Photomicrographs are oriented as in Fig. 1. Arrowheads indicate double-labelled cells. **(A-C)** A shows schematic of the experiment in B and C. Ongoing developmental neurogenesis of motor neurons (double-labelled for EdU and *mnx1:GFP*) is not different between gControl and gSema4a injected unlesioned larvae (B), quantified in C (gControl: 1.9 cells per larvae ± 0.3920; gSema4ab: 1.7 cells per larvae ± 0.3646; Mann-Whitney U-test: p = 0.5972). White boxes in B indicate quantification windows. **(D-F)** D shows a schematic of the experiment in E and F. Lesion-induced generation of motor neurons (*mnx1:GFP*+/EdU+) is increased in somatic mutants for *sema4ab* (arrowheads in E and E'-E'''). A quantification is shown in F (gControl: 6.9 cells per larva ± 0.8; gSema4ab: 12.9 cells per larva ± 1.1; Mann-Whitney U-test: p = 0.0001). (**G)** Quantifications in germline mutants for *sema4ab* show a similar increase in generation of motor neurons after lesion (wild type: 8.7 cells per larva ± 1.2; sema4ab-/-: 16.9 cells per larva ± 1.5; Mann-Whitney U-test: p = 0.0001). EdU application paradigm was as indicated in D. **(H-J)** H shows a schematic of the experiments. Overexpression of *sema4ab* driven by a heat-shock promotor (*hsp70:sema4ab*) reduces over-production of motor neurons (*mnx1:GFP*+/EdU+) back to wild type levels in *sema4ab* germline mutants, imaged in I and quantified in J (wild type: 8.5 cells per larva ± 0.95; *sema4ab* -/-: 15.4 cells per larva ± 1.2; *sema4ab*-/- + *hsp70:sema4ab*: 10 cells per larva ± 1.15; Kruskal-Wallis test: p = 0.0004; Dunn's multiple comparisons test: ***p = 0.006; n.s > 0.9999, **p = 0.0168). Error bars show SEM. Dotted lines show the injury site. Scale bars: 50 µm (B, E, I), 10 µm (E'-E''').

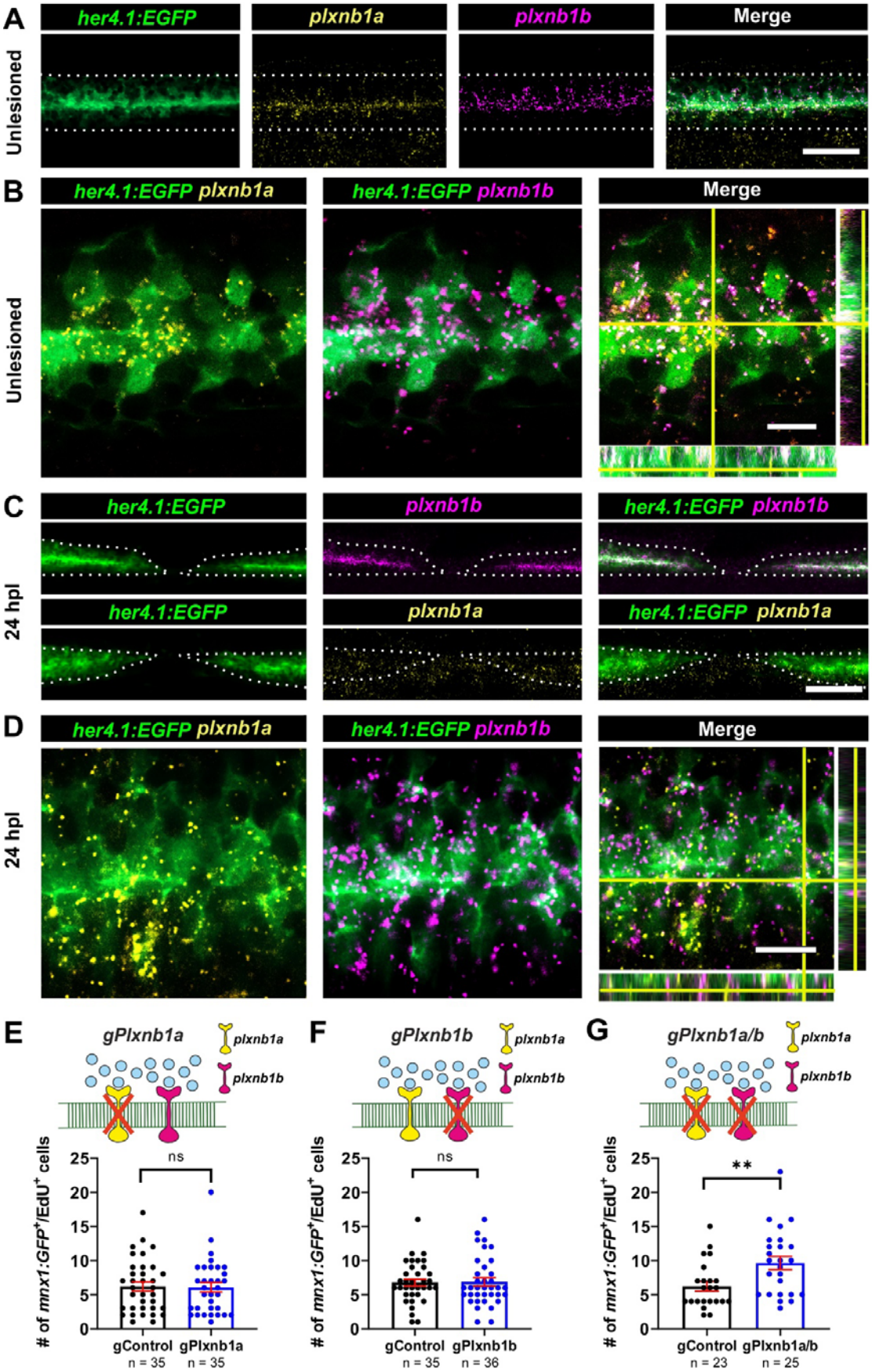
A
her4.1:EGFP
plxnb1a
plxnb1b
Merge
Unlesioned
B
her4.1:EGFP plxnb1a
her4.1:EGFP plxnb1b
Merge
Unlesioned
C
her4.1:EGFP
plxnb1b
her4.1:EGFP plxnb1b
her4.1:EGFP
plxnb1a
her4.1:EGFP plxnb1a
24 hpl
D
her4.1:EGFP plxnb1a
her4.1:EGFP plxnb1b
Merge
24 hpl
E
gPlxnb1a
plxnb1a
plxnb1b
ns
# of mnx1:GFP+/EdU+ cells
gControl
gPlxnb1a
n = 35
n = 35
F
gPlxnb1b
plxnb1a
plxnb1b
ns
# of mnx1:GFP+/EdU+ cells
gControl
gPlxnb1b
n = 35
n = 36
G
gPlxnb1a/b
plxnb1a
plxnb1b
**
# of mnx1:GFP+/EdU+ cells
gControl
gPlxnb1a/b
n = 23
n = 25

Fig. 3. *plxnb1a* and *plxnb1b* are selectively expressed by spinal progenitors and attenuate regenerative neurogenesis. Photomicrographs are oriented as in Fig. 1 **(A)** HCR-FISH in the *her4.1:EGFP* line indicate expression of *plxnb1a* and *plxnb1b* in spinal progenitor cells (*her4.1:EGFP*+) before injury**.** Dotted lines define the spinal cord extension. **(B)** High magnification showing co-localization of *plxnb1a* and *plxb1b* in *her4.1:EGFP*+ cells. **(C)** HCR-FISH in the *her4.1:EGFP* line indicates expression of *plxnb1a* and *plxnb1b* in spinal progenitor cells (*her4.1:EGFP*+) after injury**.** Dotted lines define the spinal cord extension. **(D)** High magnification showing co-localization of *plxnb1a* and *plxb1b* in *her4.1:EGFP*+ cells after injury. **(E-F)** Regenerative neurogenesis is not changed in single somatic mutants for *plxnb1a* (**E**, gControl: 6.2 cells per larva ± 0.66 ; gPlxnb1a: 6.1 cells per larva ± 0.71; Mann-Whitney U-test: p = 0.8371) and *plxnb1b* (**F**, gControl: 6.8 cells per larva ± 0.52 ; gPlxnb1b: 6.9 cells per larva ± 0.60; Mann-Whitney U-test: p = 0.6511). **(G)** Regenerative neurogenesis is increased in double somatic mutants of *plxnb1a and plxnb1b* by 55 % compared to lesioned control gRNA-injected larvae (gControl: 6.2 cells per larva ± 0.71 cells per larva; gPlxnb1a+b: 9.6 cells per larva ± 0.96; Mann-Whitney U-test: p = 0.0057). Error bars show SEM. Scale bars: 50 µm (A) 10 µm (B).

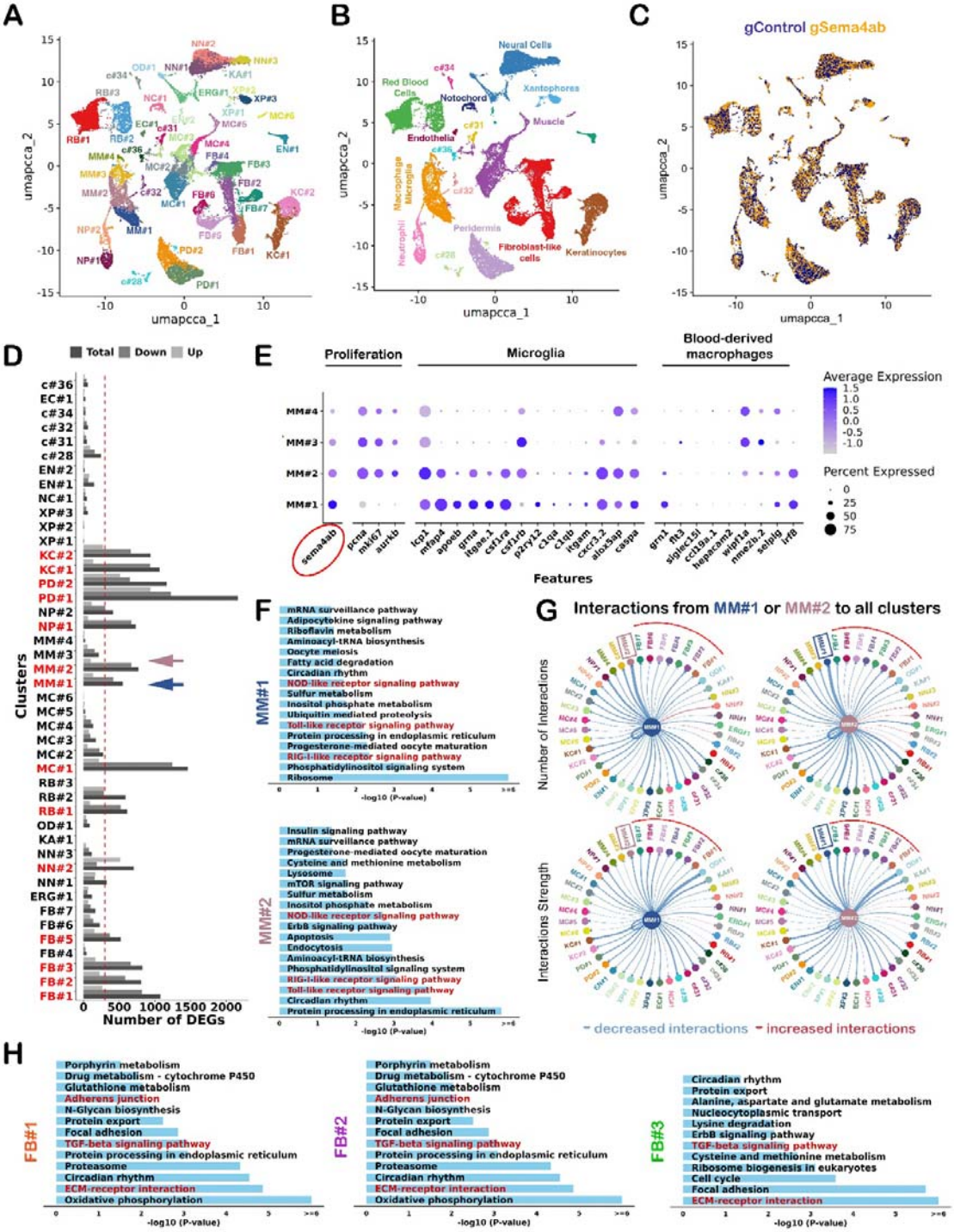
A
B
C
gControl gSema4ab
umapcca_1
umapcca_2
D
Total Down Up
Clusters
Number of DEGs
E
Proliferation
Microglia
Blood-derived macrophages
Average Expression
Percent Expressed
Features
F
MM#1
MM#2
-log10 (P-value)
G
Interactions from MM#1 or MM#2 to all clusters
Number of Interactions
Interactions Strength
decreased interactions
increased interactions
H
FB#1
FB#2
FB#3
-log10 (P-value)

Figure 4. scRNAseq indicates changes in cell interactions between macrophages and other cell types. (A,B) Cluster analysis identifies 44 cell clusters (A) that represent the main expected cell types (B) in the injury site at 24 hpl. **(C)** A plot comparing cell numbers between samples shows no major changes in cell type representation resulting from *sema4ab* disruption (gControl in blue, gSema4ab in yellow). **(D)** A graph indicating differential expression of genes (DEG) between samples is shown. Cell clusters with major changes (>300 DEGs) are indicated in red. Arrows point to macrophage clusters (MM#1 and MM#2). **(E)** A dot plot of the 4 macrophage clusters depicting the expression levels of *sema4ab* and the indicated cell type marker genes. **(F)** KEGG analysis of MM#1 and MM#2 clusters shows changes in macrophage activation pathways (highlighted in red). **(G)** CellChat analysis for macrophage clusters MM#1 and MM#2 shows interactions with all cell types and a general decrease in these interactions (blue lines) when *sema4ab* is disrupted. Note that these clusters are also highly interactive between each other (box) and with fibroblast-like cells (indicated by curved red line). **(H)** KEGG analysis of the signalling pathways most affected by *sema4ab* disruption in fibroblast-like cell clusters (FB#1, FB#2 and FB#3) is shown. Common pathways are indicated in red.

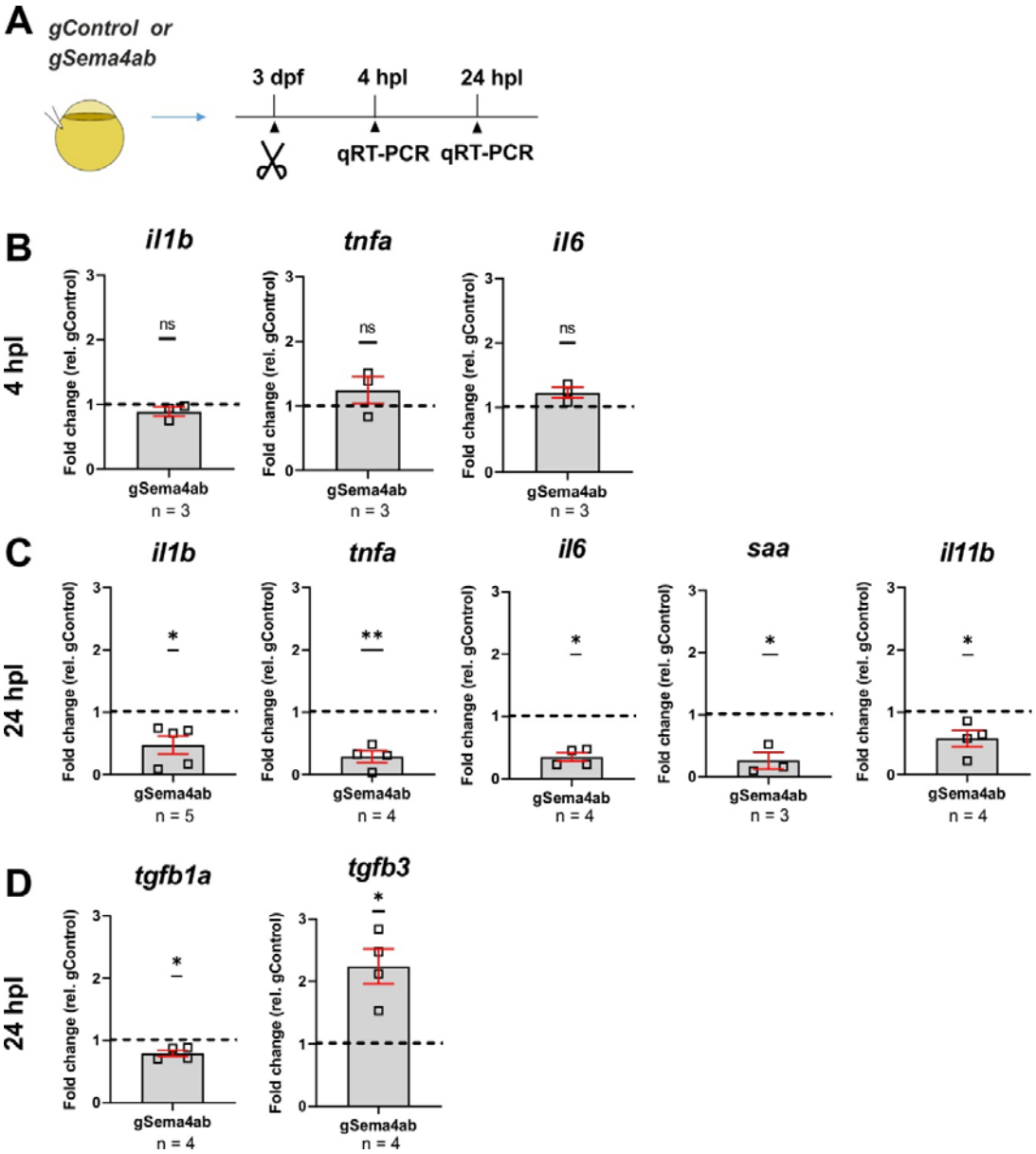
A
gControl or
gSema4ab
3 dpf
4 hpl
24 hpl
qRT-PCR
qRT-PCR
B
4 hpl
il1b
tnfa
il6
Fold change (rel. gControl)
ns
gSema4ab
n = 3
C
24 hpl
il1b
tnfa
il6
saa
il11b
*
**
gSema4ab
n = 5
n = 4
n = 4
n = 3
n = 4
D
24 hpl
tgfb1a
tgfb3
gSema4ab
n = 4
n = 4

Fig. 5. Loss of *sema4ab* function changes the cytokine profile of the injury site. (A) A schematic indicating the experimental design for cytokine quantification by qRT-PCR is shown. **(B)** qRT-PCR analyses of major pro-inflammatory cytokines in *sema4ab* somatic mutants show no differences to injured control gRNA-injected larvae at 4 hpl (peak of neutrophil response; *il1b*: p = 0.2526; *tnfa*: p = 0.3623; *il6*: p = 0.1028)**. (C)** At 24 hpl, *sema4ab* somatic mutants show decreased expression levels of pro-inflammatory cytokines (*il1b*: -2.12 fold-change, p = 0.0212; *tnfa*: -3.58 fold-change, p = 0.0047; *il6*: -2.94 fold-change, p = 0.0024; *saa*: -3.84 fold-change, p = 0.0311; *il11b*: -1.73 fold-change, p = 0.0495). **(D)** While the anti-inflammatory cytokine *tgfb1a* shows a slight decrease (-1.26 fold-change, p = 0.0251), *tgfb3* is substantially increased in expression in *sema4ab* somatic mutants (+2.24 fold-change, p = 0.0210). Statistical tests: One-sample t-test. Each dot represents a pool of 50 larvae. Error bars show SEM.

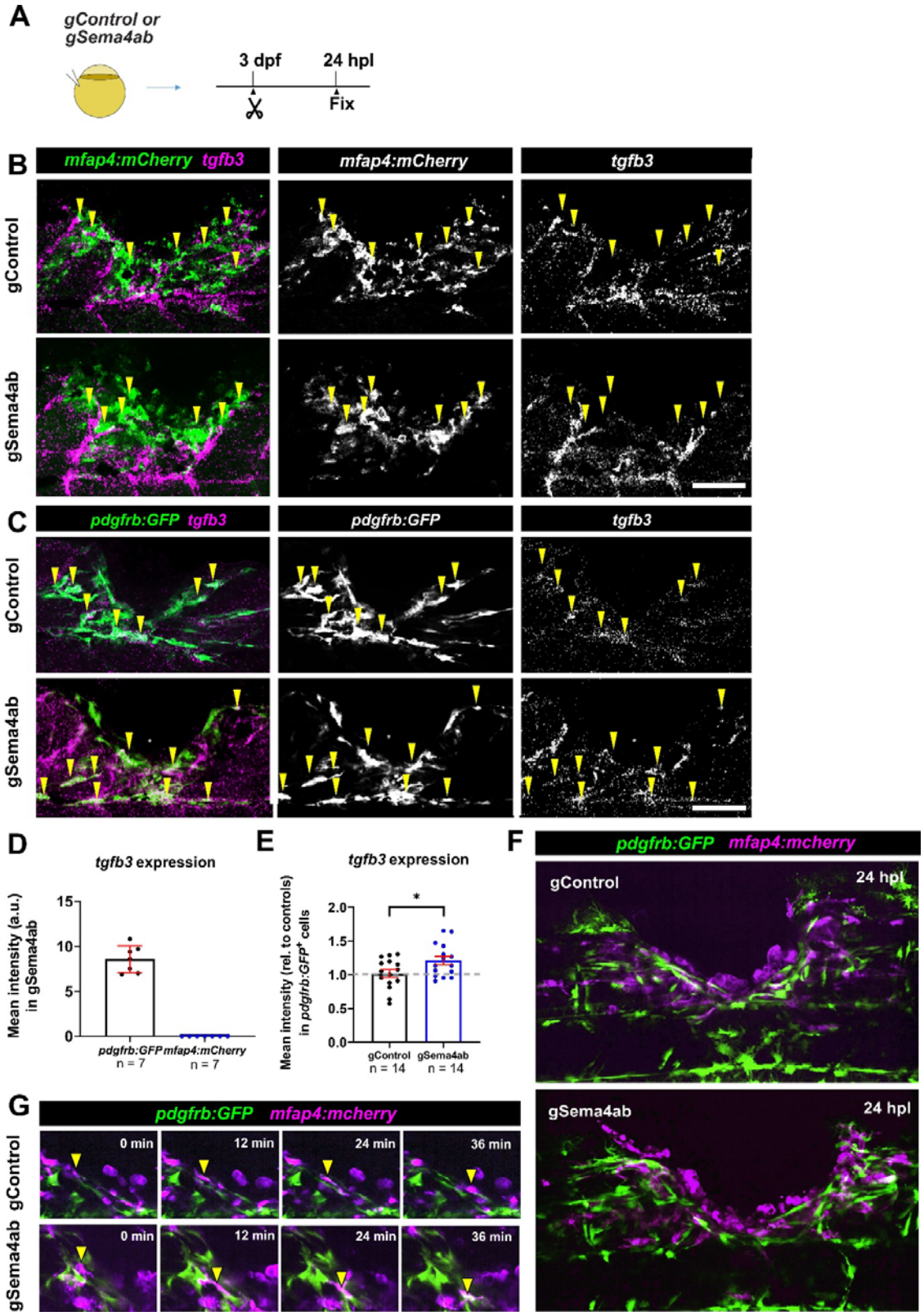
A
gControl or gSema4ab
3 dpf
24 hpl
Fix
B
mfap4:mCherry tgfb3
mfap4:mCherry
tgfb3
gControl
gSema4ab
C
pdgfrb:GFP tgfb3
pdgfrb:GFP
tgfb3
gControl
gSema4ab
D
tgfb3 expression
Mean intensity (a.u.) in gSema4ab
15
10
5
0
pdgfrb:GFP n = 7
mfap4:mCherry n = 7
E
tgfb3 expression
Mean intensity (rel. to controls) in pdgfrb:GFP+ cells
2.0
1.5
1.0
0.5
0.0
*
gControl n = 14
gSema4ab n = 14
F
pdgfrb:GFP mfap4:mcherry
gControl
24 hpl
gSema4ab
24 hpl
G
pdgfrb:GFP mfap4:mcherry
gControl
gSema4ab
0 min
12 min
24 min
36 min

Fig. 6. Fibroblasts increase *tgfb3* expression in the absence of *sema4ab* function. (A) A schematic indicating the experimental design for B-E is shown. **(B)** Multiplexed HCR-FISH at 24 hpl shows no detectable *tgfb3* signal in macrophages (*mfap4:mCherry*$^{+}$; arrowheads) in lesioned animals with or without *sema4ab* disruption. **(C)** Multiplexed HCR-FISH at 24 hpl shows *tgfb3* expression in fibroblast-like cells (*pdgfrb:GFP*$^{+}$; arrowheads) with or without *sema4ab* disruption. **(D)** Quantification of mean intensity of the *tgfb3* signal shows expression in *pdgfrb:GFP*+ cells but no detectable signal in *mfap4:mCherry*+ cells in *sema4ab* haCR-injected larvae. **(E)** Comparing mean intensity of the relative fluorescence for the *tgfb3* signal in *pdgfrb:GFP*$^{+}$ cells between control gRNA-injected and *sema4ab* haCR-injected larvae shows an increase of the *tgfb3* signal in fibroblasts in *sema4ab* haCR-injected larvae at 24 hpl (gControl: 1.01 a.u. ± 0.058; gSema4ab: 1.22 ± 0.063; t-test: $p = 0.0322$). **(F)** Individual frames of time-lapse movies show *mfap4:mCherry* positive cells in close contact to *pdgfrb:GFP* positive cells in both control gRNA injected and in *sema4ab* somatic mutant fish. **(G)** Time series of movie frames show that macrophages (arrow) migrate along fibroblast processes in both conditions. Error bars show SEM. Scale bars: 50 µm.

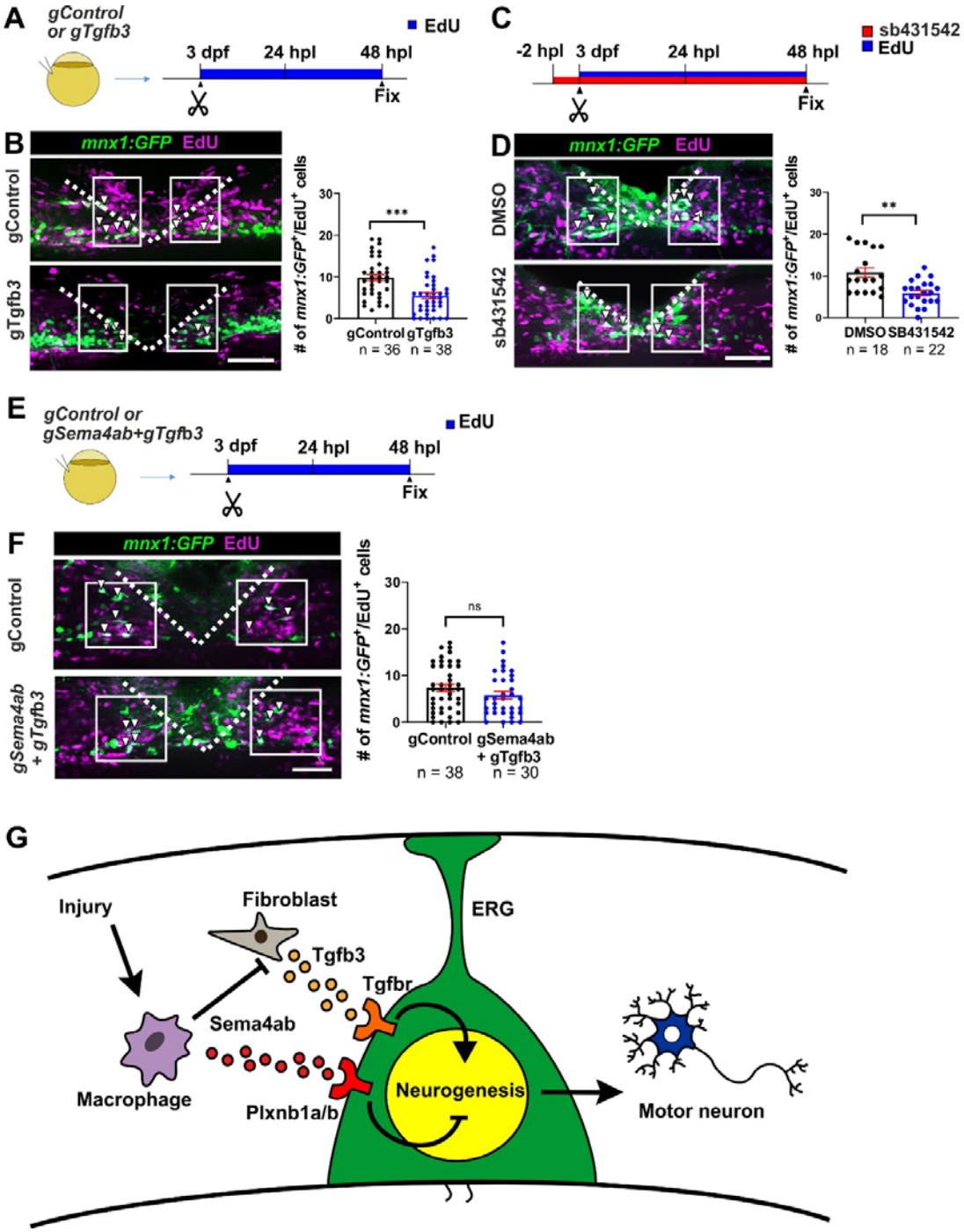
A
gControl or gTgfb3
EdU
3 dpf
24 hpl
48 hpl
Fix
B
mnx1:GFP EdU
gControl
gTgfb3
# of mnx1:GFP+/EdU+ cells
***
gControl gTgfb3
n = 36 n = 38
C
-2 hpl
3 dpf
24 hpl
48 hpl
sb431542
EdU
Fix
D
mnx1:GFP EdU
DMSO
sb431542
# of mnx1:GFP+/EdU+ cells
**
DMSO SB431542
n = 18 n = 22
E
gControl or gSema4ab+gTgfb3
EdU
3 dpf
24 hpl
48 hpl
Fix
F
mnx1:GFP EdU
gControl
gSema4ab + gTgfb3
# of mnx1:GFP+/EdU+ cells
ns
gControl gSema4ab + gTgfb3
n = 38 n = 30
G
Injury
Fibroblast
ERG
Tgfb3
Tgfbr
Sema4ab
Macrophage
Plxnb1a/b
Neurogenesis
Motor neuron

Fig. 7. Fibroblasts promote regenerative neurogenesis via *tgfb3*.

(A,B) A schematic timeline of the experimental design is shown (A). Somatic mutants for *tgfb3* show a reduction in the number of newly generated motor neurons (B, gControl: 9.8 cells per larva ± 0.8; gTgfb3: 5.5 cells per larva ± 0.7; p = 0.0001). **(C,D)** A schematic of the experimental design is shown (C). Drug treatment using the small molecule inhibitor SB431542 against Tgfb-receptors mimics reduction in regenerative neurogenesis observed with *tgfb3* somatic mutants (D, DMSO: 10.8 cells per larva ± 1.15; SB431542: 5.9 cells per larva ± 0.63; p = 0.0011). **(E,F)** A schematic timeline for double gene disruption is shown (F). Double haCR injection against *sema4ab* and *tgfb3* restores control levels of regenerative neurogenesis (gControl: 8.1 cells per larva ± 0.7; gSema4ab+gTgfb3: 6.6 cells per larva ± 0.8; p = 0.1523). **(G)** A graphical summary of proposed interactions of *sema4ab* during spinal cord regeneration is shown. After spinal injury, macrophages likely control neurogenesis directly by signalling through Sema4ab and Plxnb1a/b on ERGs and indirectly by controlling expression of *tgfb3*, a positive regulator of regenerative neurogenesis, in fibroblasts. Error bars show SEM. Dotted lines show the injury site. Scale bars: 50 µm.

TABLES

Top 10 downregulated genes in macrophages (gSema4ab vs gControl)							
Ensembl ID	**Gene Symbol**	**p_val**	**avg_log2FC**	**pct.1**	**pct.2**	**p_val_adj**	**Fold Change**
ENSDARG00000057789	lyz	4,6621E-14	-2,90	0,325	0,442	1,2211E-09	-7,47
ENSDARG00000089362	grn1	1,4603E-20	-2,72	0,22	0,353	3,8248E-16	-6,57
ENSDARG00000109929	ITGB1	2,1781E-45	-2,13	0,137	0,352	5,7048E-41	-4,39
ENSDARG00000026049	mxf	8,8469E-10	-1,94	0,168	0,252	2,3172E-05	-3,83
ENSDARG00000074995	eif2b5	1,0336E-17	-1,93	0,061	0,156	2,7072E-13	-3,81
ENSDARG00000099719	cdkn1d	2,5513E-19	-1,90	0,025	0,102	6,6822E-15	-3,73
ENSDARG00000100442	cfh	4,1416E-11	-1,90	0,097	0,178	1,0848E-06	-3,72
ENSDARG00000037618	ddit4	7,2773E-08	-1,86	0,066	0,122	0,00190607	-3,62
ENSDARG00000037121	mat2ab	4,3434E-11	-1,83	0,095	0,175	1,1376E-06	-3,56
ENSDARG00000112593	hist1h2a3#31448	6,1688E-09	-1,77	0,084	0,15	0,00016157	-3,40

Table 1. Top 10 downregulated genes in all macrophages after sema4ab somatic mutation in scRNAseq.